2009-01-01

Integrated Finite Element Analysis Program to Evaluate Pavement Performance and Predict Non-Destructive Testing Response

Cesar Tirado
University of Texas at El Paso, ctirado@miners.utep.edu

INTEGRATED FINITE ELEMENT ANALYSIS PROGRAM TO EVALUATE PAVEMENT PERFORMANCE AND PREDICT NON-DESTRUCTIVE TESTING RESPONSE

CESAR TIRADO

Department of Civil Engineering

APPROVED:

Cesar Carrasco, Ph.D., Chair

Soheil Nazarian, Ph.D.

Carlos Ferregut, Ph. D.

John F. Chessa, Ph.D.

Patricia D. Witherspoon, Ph.D.
Dean of the Graduate School

This dissertation is dedicated to

my beloved wife, Ana María Aguirre

my parents, Guillermina Díaz Mendoza and César Tirado Villegas,

who supported and encouraged me throughout my studies,

and to Pelucho and Chiquita

for their company along the way.

INTEGRATED FINITE ELEMENT ANALYSIS PROGRAM TO EVALUATE PAVEMENT PERFORMANCE AND PREDICT NON-DESTRUCTIVE TESTING RESPONSE

by

CESAR TIRADO, B.S.C.E., M.S.C.E.

DISSERTATION

Presented to the Faculty of the Graduate School of

The University of Texas at El Paso

in Partial Fulfillment

of the Requirements

for the Degree of

DOCTOR OF PHILOSOPHY

Department of Civil Engineering

THE UNIVERSITY OF TEXAS AT EL PASO

December 2009

Acknowledgements

I would like to thank my committee chairman, Dr. Cesar Carrasco, and to Dr. Soheil Nazarian, director of the Center for Transportation Infrastructure Systems (CTIS), for their advice, guidance and support throughout my doctoral studies. My sincere appreciation is extended to the committee members, Dr. Carlos Ferregut and Dr. Jack Chessa for their help and comments.

Special appreciation is extended to the Center for Infrastructure Systems (CTIS), whose project for developing IntPave, the Integrated Pavement Damage Analyzer, was sponsored by the New York Department of Transportation and the Texas Department of Transportation, and particularly the people who have been involved in its development and implementation: Imad Abdallah, José Mares, Yan Qing, Manuel Celaya, Enrique Portillo and Shahram Misaghi. Furthermore, I would like to express my gratefulness to all professors, staff, and graduate students of the Department of Civil Engineering for their help and assistance. Specially, I would like to thank Dr. Gilberto Wenglas, Dr. Yaqi Wanyan, Daniel Velazco, Andrés Franco, Porfirio Peinado and Fernando Astorga for their unconditional friendship and support.

I would like to thank my beloved wife Ana María Aguirre and my parents, César Tirado Villegas and Guillermina Díaz Mendoza for their moral support and encouragement during my studies.

Abstract

The response of a pavement system under wheel loading has been a subject of research for many decades. Several models have been developed to predict pavement performance based on layer deformation and fatigue cracking. Among them stand out computer programs based on linear elasto-static layered systems and viscoelastic-plastic models; however, newer or more advanced constitutive models cannot be rigorously incorporated into them. In contrast, finite element techniques allow incorporation of nonlinear and viscoelastic-plastic behavior of the pavement materials but licensing of software and the need to train personnel greatly limits its use by highway agencies. A mechanistic-empirical (M-E) approach for the estimation of pavement performance is proposed and implemented into a software package called Integrated Pavement Damage Analyzer (IntPave). The program has the capacity of calculating pavement distresses, i.e. rutting and fatigue cracking, for flexible pavements under any type of traffic load using finite element analysis. On the other hand, damage equivalency has been defined by AASHTO based on an empirical approach, thus being necessary a more rational approach to estimate damage based on mechanistic-empirical models. Such methods are proposed for the determination of damage factors using IntPave to allow the comparison the level of distress caused by a heavy truck relative to a standard truck. Furthermore, a process based on the M-E models was developed to estimate permit fees based on the predicted pavement deterioration that a truck causes. Case studies are presented to evaluate damage caused by both legal and overweight trucks and by trucks with similar gross vehicle weights but different axle configurations, as well as determining the effect on the permit fee.

Table of Contents

List of Figures

Page

List of Tables

Page

Chapter 1

Introduction

1.1 General

Pavements are typically subjected to traffic loading and temperature conditions that lead to their deterioration during their design lives. Pavement management decisions must be implemented by transportation agencies that seek to address this issue by gathering information about the pavement conditions, its analysis and forecast, and possible preventive maintenance or rehabilitation. In order to study the pavement performance, the response of a pavement system under wheel loading has been a subject of research for many decades. Various experiments were carried out which the AASHO Road Test stands out, a late 1950's $27 million investment which happened to be the largest road experiment of its time. This test program was conceived and sponsored by the American Association of State Highway Officials (AASHO) to study the performance of highway pavement structures of known thickness under moving loads of known magnitude and frequency (AASHO 1961). Such study became a primary source of experimental data of vehicle damage to highways for the purposes of road design, vehicle taxation and costing. From such tests, empirical derived equations were presented in the 1986 AASHTO pavement design guide.

Present pavement and traffic conditions exceeded data limits and conditions used in the AASHTO Road Test because empirical design processes restricted pavement performance prediction; thus, a suitable mechanistic pavement analysis and design procedure was necessary for future versions of the AASHTO guide. In order to address the need of this new method, the

National Cooperative Highway Research Program (NCHRP) developed a new pavement design and analysis tool called The Mechanistic-Empirical Design Guide for New and Rehabilitated Pavement Structures (ERES Consultants, Inc. 2004). Newer techniques based on mechanistic analysis were further developed to study pavement performance; several computer programs have been developed to analyze the structural response of pavement systems based on layered theory or empirical equations.

1.2 Problem statement

The implementation of the North American Free Trade Agreement (NAFTA) among Canada, Mexico, and the United States has called the attention of some state departments of transportation along the border to understand the impact of heavier axle loads and new axle configurations on their highway networks. Highways designed to carry vehicle loads of 80 kips (350 KN) could be trafficked with gross vehicle loads of over 120 kips (500 KN), by trucks with different tire and axle configurations. For example, specialized haulage vehicles in Mexico are equipped with "super-single" tires, and tridem-axles and triple trailers are used on many long haul routes in Canada. The use of these heavy loads and new vehicle configurations will have a major impact on the performance of the U.S. highway network. Hence, highway agencies urgently need tools to predict the additional damage and the economic impacts of allowing such trucks in the U.S. highway system.

Over the years, some programs for calculating pavement response were made available and distress models were developed to predict pavement performance due to loading. A number of computer programs have been developed to calculate stresses based on linear elasto-static layered systems, such as BISAR, ELSYM5, and WESLEA, as well as viscoelastic-plastic

programs such such as VESYS (Kenis 1977; Zhou and Scullion 2002). However, despite the success of these models, new or more advanced constitutive models cannot be rigorously incorporated into them. Commercial software based on Finite Element Modeling (FEM) with the capacity to comprehensively model pavement damage also exists. These software packages have a steep learning curve and in general are not user friendly. Thus, newer and simplified tools must be developed to address the need to analyze pavements and provide a forecast of damage based on a mechanistic analysis while also being user friendly and cost effective.

The use of a FEM core in the development of a pavement analysis tool provides an excellent solution for the analysis of pavement performance as long as it is capable of reducing to a minimum the level of knowledge the user needs to have of the FE method. Such FEM program would even be useful for addressing the need of assisting the nondestructive evaluation of pavements.

The need for evaluating the structural capacity of pavements while minimizing traffic interruption to a minimum testing time prompted the development of nondestructive pavement testing techniques. Many of these methods involve deflection methods, ground-penetrating radar, impact hammer and wave propagation devices. Seismic methods, i.e. wave propagation methods, meet the requirements for rapid testing and are suitable for evaluating the structural integrity of layered pavement systems to determine the remaining service life of a pavement or its load-carrying capacity. The Spectral Analysis of Surface Waves (SASW) method is a technique used for examining the structural integrity of pavement systems. This method outperforms other nondestructive evaluation methods given that it only needs access from one side of the testing object and it can measure the dispersive characteristics in layered structures. This technique consists in generating and measuring stress waves, i.e. Rayleigh waves that

propagate along the surface. Its objective consists in obtaining the Rayleigh wave dispersion curve to ultimately obtain the shear wave velocity profile in order to determine the elastic parameters and layer thicknesses. However, this last part requires a backcalculation or inversion process, also called inversion mapping, to find a theoretical layered system having a dispersion curve (called a theoretical dispersion curve) that closely matches the previously obtained experimental one. Unfortunately, profile properties cannot be formulated as a function of the dispersion characteristics of the system, resulting in a non-linear and non-unique solution. To accomplish this step, manual trial and error procedures, both complicated and time-consuming, have been employed. These procedures require in addition specialist expertise to perform this task effectively. Automated processes have been developed to rapidly determine the stiffness profiles. Numerical modeling in the form of the finite element method has been used to validate its testing results. Researchers have been using a variety of commercial finite element analysis programs to simulate wave propagation for nondestructive evaluation, such as ABAQUS and ANSYS, for pavement characterization and determination of cavities in flexible pavements. However, both the licensing of the programs and the necessity for training personnel to manage them makes them difficult to implement, especially when a limited budget is available. Moreover, it has been found that finite element analyses, despite its advantages, are computationally expensive and more time consuming than other wave propagation in layered media theory based methods (Ganji *et al*. 1998). Thus, simpler and inexpensive tools developed specifically for the analysis of pavements are required using FEM.

1.3 Objectives

The main objective of the research carried on and explained in this dissertation consists on the development of a methodology to assess the impact of heavy and super-heavy trucks on pavements based on a mechanistic-empirical analysis. To obtain the pavement performance a FEM program called IntPave, an Integrated Pavement Damage Analyzer, was developed. Such program developed by Tirado *et al.* (2007), integrated a finite element analysis code that has the capability of analyzing pavement sections using two- and three-dimensional models, and is based on generalized Hooke's law to model the properties of pavement structure. In order to assess the impact heavy trucks cause, a comparison analysis is performed based on the distresses caused. To achieve such purpose a new procedure is proposed to analyze the effect truck traffic on pavement deterioration by integrating the effect of all axles comprising a truck into a truck pass, rather than focusing on axle groups. Furthermore, the effect of a truck passage is evaluated with respect to a standard truck to evaluate the extra damage caused by such truck. Such comparative analysis is used to propose a procedure based on a mechanistic-empirical (M-E) analysis to estimate permit fees based on a truck axle loading and configuration and the predicted pavement deterioration it causes. Moreover, this program can be modified adequately to allow the inclusion of a time integration of the equation of motion suitable for solving the wave propagation problem. Numerical results obtained through the finite element method would serve as guide to seismic testing techniques.

Chapter 2

Pavement Distresses

2.1 Introduction

Pavement distress information is important to engineers in designing pavement systems and managing highway networks. As pavements age and experience traffic loads, pavement distresses begin to accumulate. Common types of pavement distresses include cracking, distortion and disintegration, leading to deterioration that can cause vehicle hazards. Typical causes of pavement deterioration include traffic loading, environmental conditions and construction deficiencies. Distresses can compound themselves leading to a further rapid deterioration of the pavement; therefore, timely maintenance must be carried to maintain the pavement in serviceable conditions.

In the case of asphalt pavements different types of distresses may occur: alligator or fatigue cracking, block cracking, lane and shoulder dropoff or heave, longitudinal and transverse cracking, pumping and water bleeding, rutting, swelling, bleeding, corrugation, depression, potholes, patch deterioration, aggregate polishing, raveling and weathering.

Fatigue cracking, also called alligator cracking, is considered a major structural distress, and it happens when a series of interconnected cracks develop due to fatigue failure of the HMA surface (or stabilized base) under repeated traffic loading. Cracking initiates at the bottom of the asphalt surface or stabilized base, where tensile stress or strain is highest under a wheel load, and propagates towards the surface forming longitudinal parallel cracks, in a process also called “bottom-up” cracking (Huang 2004), as shown in Figure 2.1. As traffic continues, these cracks connect forming sharp-angle pieces, less than 30 cm (1 ft) on their longest side, which resemble the skin of an alligator, as shown in Figure 2.2. These cracks appear only in areas subjected to

traffic loading, i.e. under the wheel paths. As a result, this type of distress leads to moisture infiltration, roughness, and may even deteriorate to a pothole.

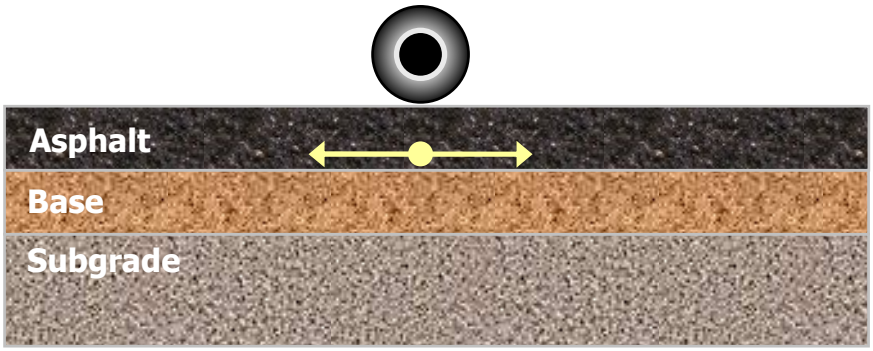

Figure 2.1 – Pavement cross section depicting maximum tensile strains occurring on the bottom of the asphalt pavement due to loading that cause fatigue cracking process.

Figure 2.2 – Pavement alligator cracking due to heavy loads on SR-532, near IH-5, Washington State (WSDOT 1996).

Rutting is a phenomenon that presents itself as a depression in the wheel path which may be accompanied by pavement uplift occurring along the sides of the rut, as shown in Figures 2.3 and 2.4. It develops from a permanent deformation in any of the pavement layers or in the subgrade caused by consolidation or lateral movement of the materials due to traffic loading or by plastic movement of the asphalt mix due to hot weather or inadequate compaction during

construction (Huang 2004). Significant rutting can lead to major structural failure and is more noticeable when filled with water after rainfall that may lead to hydroplaning.

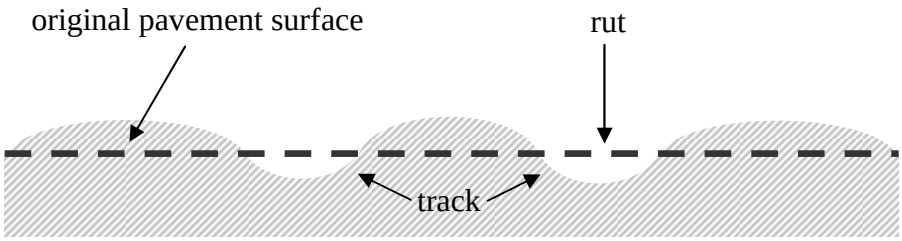

Figure 2.3 – Pavement cross section showing rutting under the wheel path.

Figure 2.4 – Rutting under the wheel path (Washington Asphalt Pavement Association 2002).

Pattern-type cracking happening in areas not subjected to loading is called block cracking and, unlike fatigue cracking, it is not related to loading but to shrinkage of HMA due to daily temperature variation causing cyclic stress and strain. Rectangular pieces (blocks) range in size from 0.1-9 m^2 (1-100 ft^2). Swelling happens when the pavement surface protrudes upward sharply or gradually forming a wave developing some cracking on the surface. It is caused by frost heave in the subgrade or by swelling soils. Bleeding develops on the pavement surface due

to high asphalt or low air void content, accumulating a film of bituminous material appearing as a shiny reflecting and sticky surface. Corrugation develops due to plastic movement forming ripples along the surface due to shear caused by vehicles acceleration or deceleration. Depression forms by settlement of the underlying soil causing roughness and may fill with water. Lane or shoulder joint separation happens when joints widen. Patch deterioration occurs over areas where the original pavement is replaced. Polished aggregates happen under wheel path due to repeated traffic loading reducing skid resistance. Potholes develop on the pavement surface that are caused by fatigue cracking, localized disintegration or freeze-thaw cycles.

Evaluation of pavement performance is important for pavement design, rehabilitation, and management. Different pavement performance features are evaluated based on distress, roughness, friction, structure, traffic, and drainage. Evaluation greatly depends to a large extent on past experience and engineering judgment. Both expert systems and predictive models have been developed to assess pavement damage. Among the former stand out the Surface Condition Expert for Pavement Rehabilitation (SCEPTRE), developed by the Washington Department of Transportation to evaluate pavement surface distress and recommend feasible rehabilitation strategies for detailed analysis and design (Ritchie *et al.* 1986); and the Expert System for Pavement Evaluation and Rehabilitation (EXPEAR) developed by the University of Illinois for the Federal Highway Administration and the Illinois Department of Transportation which evaluates a pavement section and rehabilitation alternatives (Hall *et al.* 1989). On the other hand, various predictive models based on regression analysis have been developed to predict performance of flexible pavement systems. In the following section a brief overview of predictive models is shown that addresses the major types of distress for flexible pavements, i.e. rutting and fatigue cracking.

2.2 Rutting

Permanent deformation is considered a major distress in flexible pavements. Various methods have been developed for determining permanent deformation and are based on material parameters that must be obtained based on experimental methods. Most methods make use of a repeated-load test, similar to the resilient modulus test, where permanent deformations, i.e. rut depths, are recorded based on a given number of designated cycles that may reach 100,000 repetitions.

VESYS (Kenis, 1977; FHWA, 2003) and the new Mechanistic-Empirical Pavement Design Guide (ERES Consultants, Inc., 2004) model rutting progress using a constitutive model in the form,

$$\varepsilon_p = \frac{\mu}{1-\alpha} \cdot \varepsilon_r \cdot N^{1-\alpha} \tag{2.1}$$

where ε_p is the accumulated permanent strain, ε_r is the resilient elastic strain, N is the load cycle number and α and μ are the rate of increase in permanent deformation against the number of load applications and the permanent deformation, respectively, which are material parameters measured in the laboratory.

The resilient elastic strain within a pavement layer is simply the total compression of that layer, given by the difference in deflections of the top and bottom of the layer (FHWA 2003). For any layer this difference is written as:

$$R_D(N) = \int_{N_1}^{N_2} U \cdot \mu \cdot N^{-\alpha} dN\,, \tag{2.2}$$

where R_D is the rut depth at the N^{th} load repetition and U is the layer elastic deflection. This equation may be rewritten as,

$$R_D(N) = \frac{\mu}{1-\alpha} \cdot \left(W^+ - W^-\right) \cdot N^{1-\alpha}, \tag{2.3}$$

where W^+ and W^- are the elastic deflection amplitudes of the top and bottom surfaces of the layer.

Zhou and Scullion (2002) demonstrated that α and μ are stress and temperature dependent, and as such are nonlinear. They conducted a series of lab tests on 100 mm (4 in.) diameter by 150 mm (6 in.) length cylindrical specimens. These specimens were subjected to different confining pressures, σ_3, and axial stresses, σ_1, and different temperatures to measure the permanent deformation as a function of the number of load cycles. Determination of α and μ were proposed as follows:

$$\alpha = 1.78418 - 0.446558 \cdot \log T - 2.65284 \cdot \frac{\log \sigma_d}{34.03532 - 0.253679T}, \tag{2.4}$$

$$\mu = 1.663759 - 0.438729 \cdot \log T - 1.25191 \cdot \frac{\log \sigma_d}{1.918523 + 0.066875T}, \tag{2.5}$$

where T is the pavement temperature, measured in °F, and σ_d is the deviatoric stress expressed in psi and obtained from

$$\sigma_d = \sigma_1 - \sigma_3 . \tag{2.6}$$

2.3 Fatigue cracking

To predict fatigue cracking the Asphalt Institute MS-1 model was implemented. Such model is suggested by the new MEPDG as well (ERES Consultants, Inc., 2004). Fatigue cracking is assumed to be related to tensile strain, ε_t, occurring at the bottom of the HMA layers (bottom-up cracking). The form of the load repetitions to failure of the cracking model is as follows:

$$N_f = k_1 \varepsilon_t^{-k_2} E_{ACP}^{-k_3}, \tag{2.4}$$

where N_f is the number of load applications to failure, k_1 = 0.0796, k_2 = 3.291, and k_3 = 0.854 are regression parameters based on a threshold value of 20% crack area and a typical HMA mix. Fatigue cracking predictions are calculated based on Miner's law for cumulative damage, D,

$$D = \sum_{i=1}^{T} \frac{n_i}{N_{fi}}, \tag{2.5}$$

where n_i = traffic for period i. This is later used for calculating the fatigued cracking area

$$F.C. = \left(\frac{6000}{1 + e^{C_1' + C_2' \log_{10}(100D)}} \right) \cdot \left(\frac{1}{60} \right), \tag{2.6}$$

where C'_2 = -2.40874 – 39.748 (1 + h_{ac})-2.856, C'_1 = -2 C'_2, and h_{ac} is the total thickness of the asphalt layers (ERES Consultants, Inc., 2004).

Chapter 3

Non-Destructive Testing and Evaluation

3.1 Introduction

In civil engineering practice there is a wide variety of techniques that make use of seismic methods that provide detailed information about various parameters of individual subsurface layers. Seismic methods available to civil engineers fall into two categories depending on the measured wave type: body wave and surface wave methods; both of them involve the measurement of the travel times of seismic waves. An overview of the wave propagation theory in a layered medium and a background of the seismic methods used for engineering purposes are discussed. The purpose of this section is to provide a background of the non-destructive testing techniques. Seismic techniques require a forward modeling process that would consists on the determination of the pavement layer and stiffness profile using numerical methods in order to simulate the results obtained by field testing. The dispersion curves obtained from both experimental and theoretical analyses must be matched to characterize the pavement section in order to assess the pavement performance.

3.2 Body waves

Wave motion created by a disturbance makes the particles of the medium to be displaced as the wave travels through the body of the medium. These waves are called accordingly body waves, and within an ideal whole-space they can be described by two kinds of waves: compression waves and shear waves. Compression and shear waves are distinguished by the direction of particle motion relative to the direction of wave propagation.

Compression waves, also called dilatational waves, primary waves, or *P* waves, exhibit a push-pull motion; thus, the particles of the transmitting medium move in the same direction as the waves being propagated. These waves have a higher velocity than other types of waves; consequently, they appear first in a direct travel time record. Shear waves, also called distortional waves, secondary waves or *S* waves, on the other hand, generate a shearing motion causing particle motion to vibrate perpendicular to the direction of wave propagation. As transverse waves, *S* waves exhibit polarization in both the horizontal plane, classified as *SH* waves, and in the vertical plane, classified as *SV* waves.

3.3 Surface waves

In a half-space, other types of waves occur in addition to body waves. These waves are called surface waves generally consisting of large longer-period waves, thus dominating the output of ground motion at a measuring station. Though many different types of surface waves have been identified, the two major types of waves are Rayleigh waves and Love waves. These waves propagate near the surface of the half-space.

Rayleigh waves are combination of *P* and *SV* waves that can exist at the top of a homogeneous half-space, hence they develop both a vertical and horizontal particle motion, which, when combined, form a retrograde ellipse close to the surface. As depth increases, the Rayleigh wave particle motion change gradually to pure vertical and then to a prograde ellipse. The amplitude of these waves attenuates quite rapidly with depth.

Love waves (G_n) result from the interactions of *SH* waves; hence, particle motion associated with Love waves is confined to a horizontal plane and is perpendicular to the direction of wave propagation. In contrast to Rayleigh waves, Love waves require a velocity structure that

varies with depth, and as a consequence, they cannot exit in a half-space. The simplest geometry in which a Love wave occurs is when a layer of thickness h of material with a low-velocity layer β_1 is underlain by a half-space of material with a higher velocity layer β_2, thus generating multiple reflections between the top and bottom surfaces of the low-velocity layer.

Miller and Pursey (1955) found that for the case of body and surface waves propagating away from a vertically vibrating circular source at the surface of a homogeneous, semi-infinite isotropic solid, approximately 67% of the input energy propagates in the form of Rayleigh waves, while compression and shear waves carry 7% and 25% of the energy, respectively. Both compression and shear waves propagate radially outward from the source, while Rayleigh waves propagate along a cylindrical wavefront near the surface.

3.4 Seismic wave velocity and dispersion

An important characteristic of surface waves is geometrical dispersion which arises from the fact that waves of different periods travel at different velocities in heterogeneous mediums such as earth materials. As a result, surface wave arrivals are not sharp but spread out in time. Dispersion occurs when surface waves with different periods have different displacements with depth, and the intrinsic medium velocity varies with depth, making surface wave dispersion valuable for studying the earth structure, as well as soil or pavement structures. Because dispersive waves of different frequencies propagate at different speeds, Fourier analysis is used to decompose a wave into its component frequencies for easier visualization. A plot of wave velocity versus frequency or wavelength is called a dispersion curve.

The dispersive characteristics of a wave can be demonstrated by means of either phase or group velocity. Group velocity is the velocity at which a long-period envelope wave group

propagates, whereas phase velocity is the velocity at which a carrier wave, defined by an individual high-frequency harmonic wave, travels. In a medium in which the velocity varies with frequency the long-period envelope (or wave train) changes its shape as it propagates, and, therefore, group velocity differs from phase velocity, especially when the wave propagates over a long distance. Phase velocities contain the required information to assess the material dispersive characteristics. It must be pointed out that both Rayleigh wave velocity and phase velocity are terms commonly interchangeable throughout seismic analysis for pavement engineering literature.

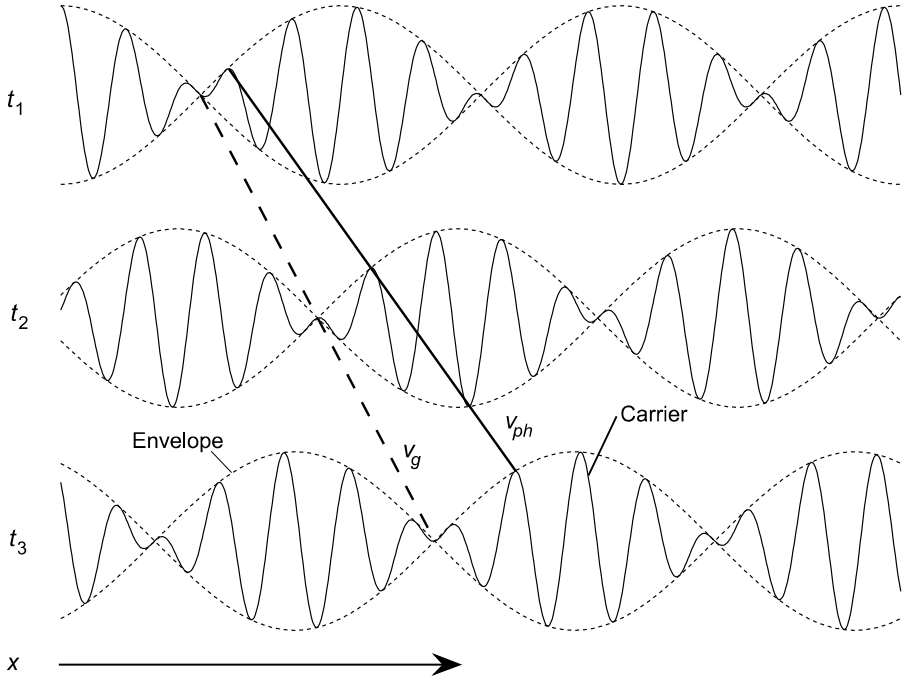

Figure 3.1 – Sinusoidal dispersive wave with long-period envelope propagating at group velocity v_g, and carrier, high-frequency wave whose amplitude is modulated by the envelope, propagating at phase velocity, v_{ph}.

The shape of a dispersion curve is affected by material's shear wave velocity, Poisson's ratio and mass density of each of the composing layers of a pavement or soil structure, as well as

their thicknesses. Solution of the dispersion function results in many roots at a given frequency called modes. The root with the smallest values is called the solution to the fundamental mode, while other solutions become higher modes. Rix (1988) assessed the relative contribution of the various modes of surface wave propagation to the overall motion using mode participation factors and determined the fundamental mode of the surface wave to compose between 72% and 86% of the total motion.

3.5 Seismic methods

Seismic methods which make use of body waves involve techniques performed entirely on the surface, like refraction and reflection methods, and techniques requiring the use of boreholes, such as crosshole and downhole methods. Surface wave methods are commonly used by seismologists to study the structure of the earth making use of the surface waves generated by earthquakes and nuclear explosions. Engineers have found these methods less popular due to involvement of bulky field equipment and empirical data analysis procedures causing significant errors; however, advancements in automation in signal recording, computer data storage and processing thus improving field instrumentation, have resulted in a wider acceptance. Surface wave testing combines the advantages of the other seismic methods, but its main advantage lies on the surface measurement of the predominant wave type of in the form of Rayleigh waves generated by a vertically-acting load source on the surface, as concluded by Miller and Pursey (1955). There is no need for boreholes, thus making it easier to test hard-to-sample materials such as gravel and loose sands and perform testing on pavements where a nondestructive evaluation is a practical requirement and where softer layers lie beneath stiffer layers (Nazarian and Stokoe 1983; Stokoe II *et al.* 1988).

Another advantage on the use of surface waves resides on attenuation, which happens for these types of waves at a smaller rate than for body waves (Ewing *et al.* 1957). Seismic waves attenuate or decrease in amplitude as they propagate through the earth due to inelasticity, also called intrinsic attenuation, which is caused by a deviation from elasticity which results from kinetic energy of elastic wave motion being lost to heat by permanent deformation of the medium (Stein and Wysession 2003). As a result of this, their energy spreads two-dimensionally and decays with distance r from the source approximately as r^{-1}, whereas the energy of body waves spreads three-dimensionally and decays approximately as r^{-2}.

3.6 Nondestructive evaluation of pavement systems

Seismic methods can be implemented for evaluating the structural integrity of pavement systems to determine the remaining service life of a pavement or its load-carrying capacity. As a practical requirement, it is necessary to evaluate the integrity of pavements using nondestructive testing to minimize traffic interruption to a minimum testing time.

One of the parameters to evaluate is the modulus of each layer. Deflection based methods have been developed and commonly used. The Dynaflect and the falling weight deflectometer (FWD) are widespread methods used in determining the stiffness of the comprising layers of a pavement structure. Both of these methods employ instruments that are deployed in a towing vehicle. The Dynaflect method consists on the application of a steady-state load to the pavement surface caused by two counter-rotating eccentric masses applying a peak dynamic force of 1,000 lb. (4,500 N) through 4-in. (10 cm) wide wheels at a frequency of 8 Hz, while deflections are read by five equally spaced geophones. In a similar way, the FWD consists on the application of an impact through a plate placed on the pavement surface which can vary

by changing drop height or weight, from 1.5–24 kips (6.6–106 kN), and an impulse duration of 25–30 ms simulating the load duration of a moving wheel at 40 mph (64 km/h), while load deflections are read by seven geophones.

Surface waves are used for comprehensive and efficient nondestructive evaluation of layered systems, such as pavements and soils. The most commonly used surface wave techniques are the Spectral Analysis of Surface Waves (SASW) and the Ultrasonic Surface Wave (USW) (Gucunski and Shokouhi 2005). These techniques have been primarily used for evaluating elastic modulus and layer thickness of layered systems. The basic assumption consists on the horizontally infinitely long and homogeneous layers of constant thickness (Gucunski and Shokouhi 2005).

3.7 Spectral analysis of surface waves (SASW) method

The spectral analysis of surface waves (SASW) method is a seismic technique founded on generating and detecting elastic stress waves. The method is based on in situ measurement of shear wave velocity and elastic moduli profile of soil sites and pavement systems at small strains, less than 0.001%; within such range of strains, moduli are independent of the strain amplitude (Nazarian 1984). Nazarian and Stokoe developed the experimental (1985) and theoretical (1986) features of the SASW method as applied to geotechnical and pavement engineering field.

Other practical applications of SASW have additionally been developed such as the measurement of the effectiveness of ground improvement at a site at which natural material was replaced by an engineered fill (Stokoe II and Nazarian 1983). Stokoe *et al.* (1988) determined shear wave velocities of hard-to-sample soils (e.g. gravelly materials and slide debris) and pavement subgrades. Rix *et al.* (1990) and Bay and Stokoe (1990) assessed the stiffness of

curing concrete with time. Similarly, Cho (2003) studied the applicability and limitations of the SASW method on high strength concrete and characterized material properties of early age high strength concrete emphasizing compressive strength.

Aouad *et al.* (1993) studied the relationship between the paving materials and temperature using SASW method finding that it is possible to quantify changes in the stiffness of the asphalt concrete surface layer with ambient temperature changes and that its moduli changes with temperature as predicted by the AASHTO guide for temperatures below 100°F (38°C). Furthermore, both small-scale laboratory tests and full-scale field studies proved that the SASW method is a viable technique for characterizing underwater geotechnical sites where soft soil-like materials are present (Luke and Stokoe II 1998).

In order for the SASW method to be practical for pavement engineering, two simplifying assumptions are required. First, the pavement structure is assumed to be comprised of horizontal layers with constant material properties. Second, only plane Rayleigh waves are involved; thus, the effect of body waves is ignored as evaluated analytically by Sánchez-Salinero (1987) and experimentally by Rix (1988), whose results proved that this is justified as long as the source-receiver spacing is kept within certain limits with respect to the wavelength.

The SASW testing process consists of three phases, starting with the field testing, followed by the determination of a dispersion curve and, finishing with the determination of the stiffness profile.

Field testing requires a test setup consisting of an impact source, two vertical geophones and a recording and analyzer device, as shown in Figure 3.2.

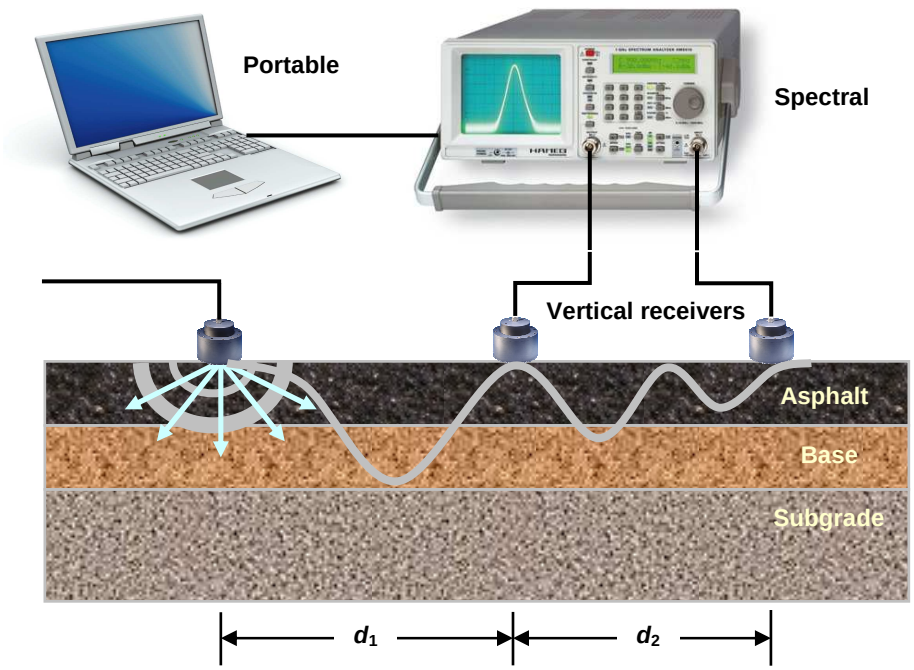

Figure 3.2 – Layout for testing setup of the SASW method.

The impact source must produce Rayleigh waves minimizing both P- and S- wave energy within an adequate frequency range. Nazarian (1984) found the highest frequencies should be within a range of 200-800 Hz for typical soil deposits, 6 kHz for flexible pavements, and 10-12 kHz for rigid pavements. Different sources have been used to generate Rayleigh waves depending on the type of material being tested and the depth to be scanned. Stokoe *et al.* (1988) summarized types of sources based on receiver spacing varying from chisels and small hand-held and sledge hammers to dropped weights. However, further developments were carried out to improve the source: Drnevich *et al.* (1985) used a vibrator connected to a random function generator; Gucunski (1991) studied impact sources capable of generating low frequency Rayleigh waves; and Nazarian *et al.* (1993) developed the Seismic Portable Analyzer (SPA), a measuring device similar to the Falling Weight Deflectometer (FWD) with a source consisting of two pneumatic hammers: one high frequency and another low frequency source, as shown in

Figure 3.4. The Seismic Portable Analyzer is capable of providing different wave propagations methods: impact echo, impulse response, SASW, ultrasonic surface waves and ultrasonic body waves.

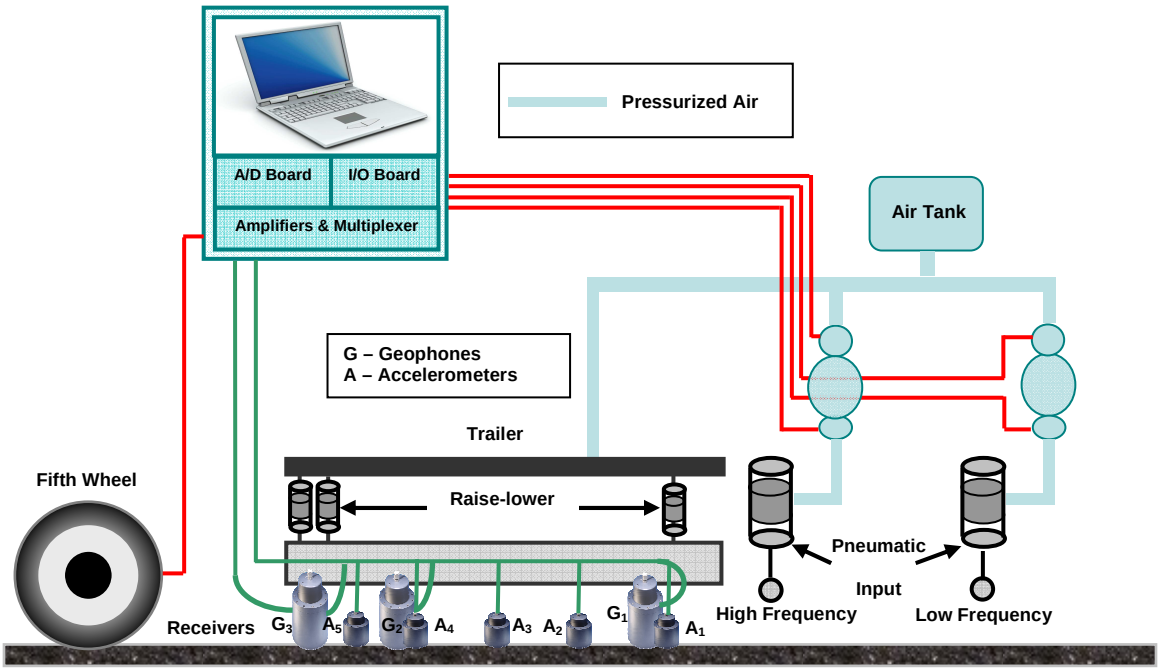

Figure 3.3 – Seismic Pavement Analyzer (SPA).

Vertically oriented velocity transducers, or geophones, and accelerometers are used in SASW testing. Geophones work within a frequency range of 1 to 1000 Hz, while the accelerometers reach 20 kHz. Pavement testing requires the use of both accelerometers and geophones, while soil testing only makes use of the latter, since accelerometers have a low output at low frequencies.

3.8 Estimation of pavement material properties

Once the dispersion curves are determined from the response obtained from the receivers of the seismic testing devices, the determination of the pavement stiffness profile is determined by making use of an iterative process that consists on proposing a pavement profile and determining if it matches the dispersion curves from the experimental testing. In order to automate the process, the forward modeling process, which consists on suggesting a pavement profile and analyzing it numerically, must be carried out using the least amount of time and resources.

A seismic forward finite element modeling code was integrated into the code of IntPave using an explicit time integration technique that greatly reduced the calculation time of the dynamic analysis. Details of the dynamic finite element analysis process are provided in the following chapter, where the modeling to analyze the pavement performance is explained.

Chapter 4

Finite Element Analysis

4.1 Introduction

Many models have been developed to predict pavement performance based on layer deformation and fatigue cracking. A number of computer programs have been developed to calculate stresses (e.g. BISAR, ELSYM5, WESLEA) based on linear elasto-static layered systems. A natural extension of layered elastic programs has been viscoelastic-plastic programs such as VESYS (Kenis 1977; Zhou and Scullion 2002). However, despite the success in these models, new or more advanced constitutive models cannot be rigorously incorporated into them. On the other hand, finite element techniques possess flexibility for incorporating nonlinear and viscoelastic-plastic behavior of the pavement materials. In order to take into account this behavior, finite element modeling software, such as ABAQUS, has been widely used. However, both the licensing of the program and the necessity for training personnel to effectively utilize these programs within highway agencies hinders its efficient utilization.

4.2 Finite element analysis of pavement systems

Finite element analysis has been commonly used to model pavement response to either static or dynamic loads yielding approximations solutions. Pavement layers are generally considered to be containing homogeneous, linear elastic and isotropic materials; however, the finite element method allows incorporating other material constitutive models like non-linear, anisotripic, stress hardening or softening models not considered in layered elastic analyses.

Furthermore, depending on the needs of the model and the required material response, finite element analyses for pavement modeling may be two-dimensional plane strain, axisymmetric, or three-dimensional, the latter being computationally expensive though more precise. Since the first implementation of the finite element method in pavements in Duncan *et al.* (1968), this method has been used to determine stresses, strains, deflections, and several other thermo-elastic and thermo-plastic responses. With the availability of computer programs and computers with faster computation time, finite element methods have gained acceptance as finite element analysis programs can handle more complex geometries, boundary conditions and material properties.

Several studies have been conducted to investigate the mechanical response of pavement to traffic. Saliba (1990) presented a brief review of the mathematical theory of visco-plasticity and the computational procedure used in a finite-element program to model tire/soil interaction. *ILLI-PAVE* is a two-dimensional axisymmetric pavement static finite element software developed at the University of Illinois at Urbana-Champaign that incorporates stress-sensitive material models and provides realistic representation of the pavement structure and its response to loading (Thompson 1989). *MICHPAVE* is a user-friendly, nonlinear finite element computer program for the analysis of flexible pavements that computes displacements, stresses and strains within the pavement due to a single circular wheel load; it accounts for stress-dependent behavior of granular and cohesive soil layers in the pavement cross section; and makes use of *K*-θ model is used to characterize the resilient moduli of granular (type 2) materials (Harichandran *et al*. 1990). Commercial finite element modeling programs like *ABAQUS* and *ANSYS* have been widely applied for pavement analysis. Chen *et al.* (1995) did a comprehensive study of pavement analysis programs, including the aforementioned, and showed that the results obtained

from *ABAQUS* were comparable to those from other programs. Zaghloul and White (1993) analyzed flexible pavements subjected to moving loads at various speeds and under FWD loading for flexible pavements using three-dimensional, dynamic analysis in *ABAQUS*. They further developed a procedure for permitting overloaded trucks in Indiana and developed load equivalency factors (LEF) for asphalt pavements with granular base as well as for full depth asphalt pavements (White and Zaghloul 1994). Tutumluer and Thompson (1997) used *GT-Pave*, a nonlinear finite element program, to compare the cross-anisotropic nonlinear elastic response to predict the performance of granular bases in flexible pavements by reducing significant tensile stresses generally predicted by isotropic linear elastic layered programs. Uddin and Ricalde (2000) implemented a viscoelastic constitutive material formulation for flexible pavements to model microcraking and crack propagation into *ABAQUS*.

Blab and Harvey (2002) used a 3-D FE model of a road pavement in which the temperature and load dependent performance of flexible pavements was characterized by a generalized Maxwell model and improved loading assumptions are used based on the required visco-elastic model parameters from dynamic shear tests. The model was evaluated using simulation calculations for a specific test structure on which rutting tests had been performed with a heavy vehicle simulator. This evaluation demonstrated good agreement between the deformations predicted by the theoretical model and the deformations actually measured.

Hossain and Wu (2002) used a three-dimensional non-linear finite element model to simulate the initiation and propagation of rutting damage on the Superpave test sections of the Kansas Accelerated Testing Laboratory. A creep and Drucker-Prager model were chosen to characterize the permanent deformation characteristics of the Superpave mixtures and the aggregate base and subgrade materials, respectively.

Werkmeister *et al.* (2003) discuss the use of shakedown approach to characterize the deformation behavior of unbound granular materials (UGM) in pavement construction. The essence of a shakedown analysis is to determine the critical shakedown load for a given pavement. The Dresden material law was introduced for modeling the permanent and resilient deformation behavior of UGM layers in pavement constructions under consideration of the shakedown ranges. They also described a design method that uses test results from the repeated load triaxial tests to establish the risk level of permanent deformations in the UGM layers using a nonlinear resilient material law implemented into a FE Program called FENLAP.

Kou and Chou (2004) developed another 3-D finite element model developed in ABAQUS for flexible pavements implementing brick finite elements and a boundary connected with infinite elements to handle an infinite boundary such as uniform subgrade without rock bed or continuous pavement in the traffic direction. Mulungye *et al.* (2005; 2006) used viscoelastic response models from ANSYS/ED finite element software to characterize the response of flexible pavements under traffic load and analyzed the dynamic response of a flexible pavement with peat foundation, in relation to tire pressure, axle load and axle configuration, considering non-linear viscoelastic characteristics of pavement material and cyclic wheel loads (Mulungye *et al*. 2007).

The Mechanistic-Empirical Pavement Design Guide (MEPDG) software utilizes two models to calculate critical responses for flexible pavements considering strains associated with traffic and climatic loading. A multi-layered linear elastic theory program called JULEA (Uzan 1989), and a non-linear axisymmetric finite element program based on DSC-2D by Desai (2001) were implemented into the MEPDG software (ERES Consultants, Inc., 2004).

Similarly, Saad *et al.* (2005) studied the dynamic pavement response of flexible pavement systems to single wheel traffic loads. The study was carried out with a finite element program called ADINA using a tree-dimensional dynamic modeling technique with implicit solution scheme. They considered the granular base as elastic perfectly plastic (Druker-Prager) and the subgrade as elastoplastic strain hardening (Cam Clay) to investigate the effect of base thickness, base and subgrade quality. Furthermore, in Saad *et al.* (2006), they implemented finite element simulations to evaluate the effect of a high modulus geosynthetic reinforcement into a pavement foundation on fatigue and rutting, and how such effects influenced base quality and thickness, as well as subgrade quality. The geosynthetic reinforcement was modeled with a isoparametric, plane stress displacement-based four-node membrane element which can lie in a three-dimensional plane, thus allowing the element for in-plane stresses and no bending nor compression stresses. The AC and subgrade were modeled with eight-node isoparametric elements.

4.3 Integrated Pavement Damage Analyzer (IntPave) finite element analysis

As part of the work conducted towards the development of this dissertation, the Integrated Pavement Damage Analyzer (IntPave) software was developed as a tool with the capacity to calculate pavement distress under any type of traffic load and to make a comparison of the level of distress caused by a standard and a non-standard truck. Such pavement distress evaluation tool consisted of three main modules: the first one was a stand-alone finite element analysis program developed in Matlab® with the capacity to load an input file and produce an output file with the pavement distress calculations. The input file contained the geometric pavement section information, material properties and their variation as a function of

temperature, and traffic loading characteristics. The output file contained the rutting calculations for all the pavement layers and fatigue cracking of the surface layer as a function of traffic load repetitions. This module was the processor (engine) used in the other two modules. The next module was a graphical user interface (GUI) that served as a pre and post processor for the stand-alone finite element program. This module provided an interface to enter all the pavement section information, material properties and traffic information in a user-friendly manner. This user interface generated an input file used by the processor, read the output and displayed the results in a graphical, easy-to-interpret form. The processor was also incorporated into a third module as a Geographic Information System (GIS)-based tool that allowed the calculation of pavement distresses and made comparisons between trucks on a road network. Instead of just doing the distress calculations at one pavement section, this tool was used to calculate the pavement distress generated by a truck as it moved through a network of roads, thus generating a "profile" of pavement distress (Tirado *et al.* 2006).

The finite element analysis was based on a generalized Hooke's law to model the properties of pavement structure. The 2D model consisted on an axisymmetric model, which was suitable for estimating the rut depth. Using an open source preprocessor called GMSH, it was possible to model a 2D mesh with triangular elements. The advantage of these elements is their geometric flexibility: they allow modeling intricate geometries and facilitate transition from coarsely meshed region of a grid to finely meshed region. This latter feature is essential in pavement modeling, since a fine mesh is required where the load is applied, implicating a larger number of elements. Since the stresses caused by loads dissipate as they move away from the load application point, a less refined mesh is needed. Even though large meshes provide more accurate results, they require greater computation time, and having these transitions greatly

reduces computation time without conceding accuracy. A sample of this type of mesh is shown in Figure 4.1. In order to improve computation time, the constant strain triangle element was used in the finite element model.

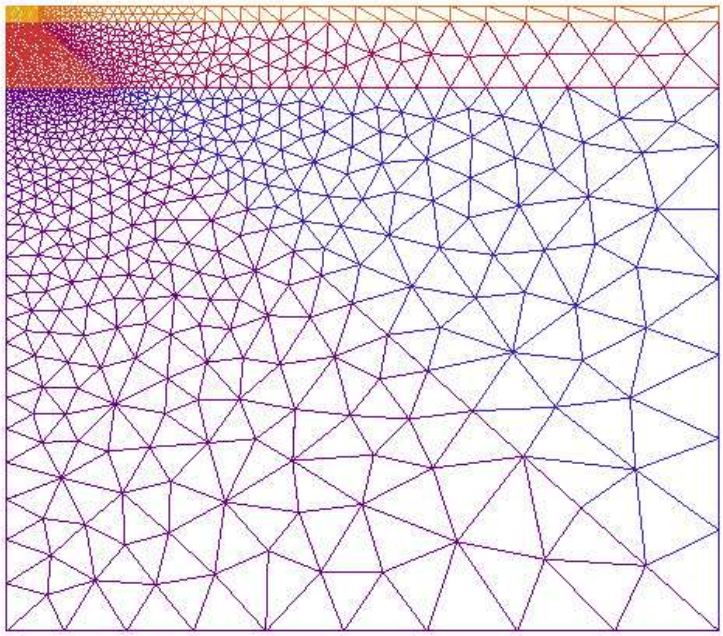

Figure 4.1 – 2D Mesh with element refinement transition, load applied at upper left corner.

Another objective of IntPave consisted on the evaluation of the impact of axle configurations to carry super heavy loads, thus making it necessary to estimate the distress using 3D modeling. Three-dimensional models offer several advantages over two-dimensional axisymmetric ones as actual load configurations can be readily modeled. These model incorporated four-node tetrahedral elements in its meshing for the same reasons the triangular element were used in the 2D model. A sample mesh of a 3D model is shown in Figure 4.2; the sample mesh becomes more refined as it gets closer to the load application points, namely the tire contact areas; in the figure shown a tandem dual axle configuration is used as an example.

Only two tires are shown in the model since only half of the model is needed because of plane symmetry.

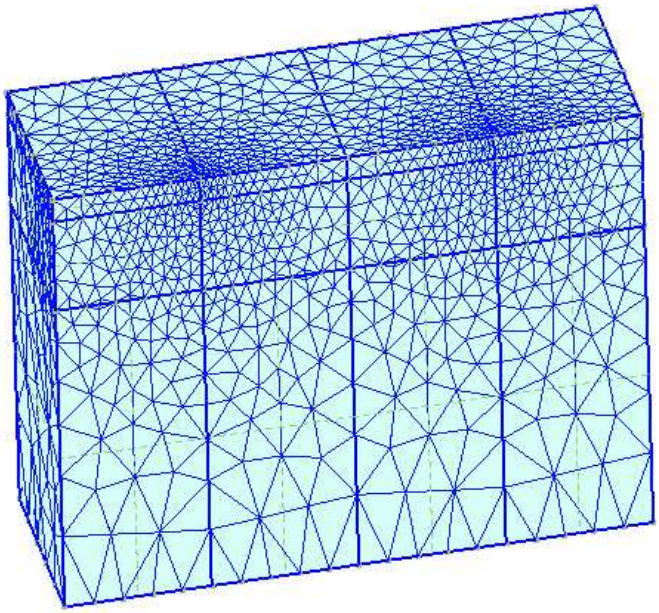

Figure 4.2 – 3D Mesh, tandem axle, dual tire load condition.

4.4 Axisymmetric stress analysis

As already mentioned, triangular elements facilitate transition from coarsely meshed zones of a grid to finely meshed zones, a feature essential in pavement modeling, as a fine mesh is required where the load is applied, but no fine mesh is necessary at regions located away from the loading, as they are not of interest to the analysis. In this section a brief explanation on the characteristics of the axisymmetric modeling is presented.

The stiffness matrix for an axisymmetric finite element analysis is computed from

$$\mathbf{K}_{ij}^{e} = \int_{V} \mathbf{B}_i^T \mathbf{D} \mathbf{B}_j dV = 2\pi \int \mathbf{B}_i^T \mathbf{D} \mathbf{B}_j r dr dz \,, \tag{4.3}$$

where **B** is the strain-displacement matrix, **D** is the elasticity matrix, r is the radial distance to the node (Zienkiewicz 1977). The strain-displacement matrix, **B**, is defined for an axisymmetric element as

$$\mathbf{B}_i = \begin{bmatrix} \frac{\partial N_i}{\partial r} & 0 \\ 0 & \frac{\partial N_i}{\partial z} \\ \frac{N_i}{r} & 0 \\ \frac{\partial N_i}{\partial z} & \frac{\partial N_i}{\partial r} \end{bmatrix}, \tag{4.4}$$

where N_i is the evaluated derivative of the shape function at node i. The interpolation functions, N_i, for the linear triangular element are shown in Table 4.1.

Table 4.1 – Interpolation functions for linear triangular elements (after Zienkiewicz, 1977).

Linear triangle	Shape functions
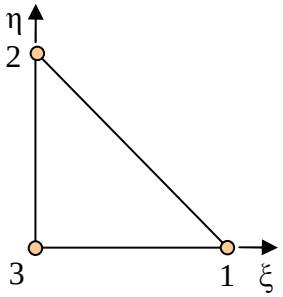	$N^1 = \xi$ $N^2 = \eta$ $N^3 = 1 - \xi - \eta$

The elasticity matrix, **D**, for an isotropic material, axisymmetric modeled, is calculated from

$$\mathbf{D} = \frac{E}{(1+\nu)(1-2\nu)} \begin{bmatrix} 1-\nu & \nu & \nu & 0 \\ \nu & 1-\nu & 0 & 0 \\ \nu & 0 & 1-\nu & 0 \\ 0 & 0 & 0 & \frac{1-2\nu}{2} \end{bmatrix}, \tag{4.5}$$

where E is the material's modulus and ν is the Poisson's ratio.

4.5 Three dimensional stress analysis

Two dimensional analyses do not allow modeling of axles, even less axle groups. Thus, a three-dimensional analysis is necessary to assess the effect an axle or an axle group might have on the pavement performance. Similar to triangular elements, tetrahedral elements allow transition from fine to coarse meshed regions. This section presents a brief explanation on the characteristics of the axisymmetric modeling.

The stiffness matrix for an axisymmetric finite element analysis is computed from

$$\mathbf{K}_{ij}^{e} = \mathbf{B}_{i}^{T}\mathbf{D}\mathbf{B}_{j}V^{e}, \tag{4.6}$$

where V^e represents the volume of the elementary tetrahedron (Zienkiewicz 1977). The strain-displacement matrix, **B**, is defined as

$$\mathbf{B}_i = \begin{bmatrix} \frac{\partial N_i}{\partial x} & 0 & 0 \\ 0 & \frac{\partial N_i}{\partial y} & 0 \\ 0 & 0 & \frac{\partial N_i}{\partial z} \\ \frac{\partial N_i}{\partial y} & \frac{\partial N_i}{\partial x} & 0 \\ 0 & \frac{\partial N_i}{\partial z} & \frac{\partial N_i}{\partial y} \\ \frac{\partial N_i}{\partial z} & 0 & \frac{\partial N_i}{\partial x} \end{bmatrix}, \tag{4.7}$$

where N_i is the evaluated derivative of the shape function at node *i*. The interpolation functions, N_i, for the linear tetrahedron element are shown in Table 4.2.

Table 4.2 – Interpolation functions for linear tetrahedron elements (after Zienkiewicz, 1977).

Linear tetrahedron	Shape functions
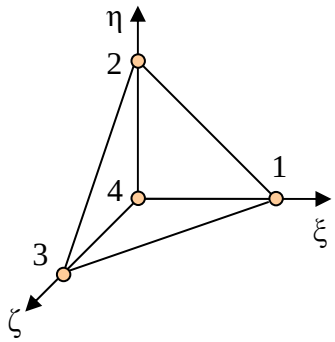	$N^1 = \xi$ $N^2 = \eta$ $N^3 = \zeta$ $N^4 = 1 - \xi - \eta - \zeta$

The elasticity matrix, **D**, for an isotropic material is calculated from

$$\mathbf{D} = \frac{E}{(1+\nu)(1-2\nu)} \begin{bmatrix} 1-\nu & \nu & \nu & 0 & 0 & 0 \\ & 1-\nu & \nu & 0 & 0 & 0 \\ & & 1-\nu & 0 & 0 & 0 \\ & & & \frac{1-2\nu}{2} & 0 & 0 \\ & \textit{Symmetric} & & & \frac{1-2\nu}{2} & 0 \\ & & & & & \frac{1-2\nu}{2} \end{bmatrix}. \quad (4.8)$$

4.6 Nonlinear model

The finite element program had the advantage of analyzing problems using either a linear analysis based on the generalized Hooke's Law, or a nonlinear analysis for both 2-D and 3-D models. For the latter approach, the nonlinear model used in the FEA program considered a load-induced nonlinear behavior based on the static linear elastic layered theory with a simple modification of the isotropic linear relation. An iterative process was employed to consider the nonlinearity of the pavement materials. The constitutive model developed by Barksdale *et al.* (1997) endorsed a universal relationship for both fine and coarse grained base and subgrade materials in the form of,

$$E = k_1 \sigma_c^{k_2} \sigma_d^{k_3} \quad (4.9)$$

where E is the resilient modulus, σ_c and σ_d are the confining pressure and the deviatoric stress, respectively; parameters k_1, k_2, and k_3 are coefficients statistically determined from the results of laboratory resilient modulus tests. The resilient modulus refers to the unloading modulus during a triaxial test in which loading, unloading and reloading are simulated under cyclic loading

conditions. A resilient modulus is defined as the ratio of the repeated deviatoric stress to the recoverable part of the axial strain. Since the state of stress can only be known if the material properties are known, an iterative process is necessary to implement this stress-modulus relationship shown in Equation 4.9. In order to implement an iterative process to obtain the non-linear resilient modulus for base and subgrade materials while keeping the asphalt modulus linear, a discriminating process was set between elements subjected to linear and nonlinear analyses, thus the asphalt layers were not included in this nonlinear behavior and, therefore, were excluded from the iterative process, as shown in Figure 4.3.

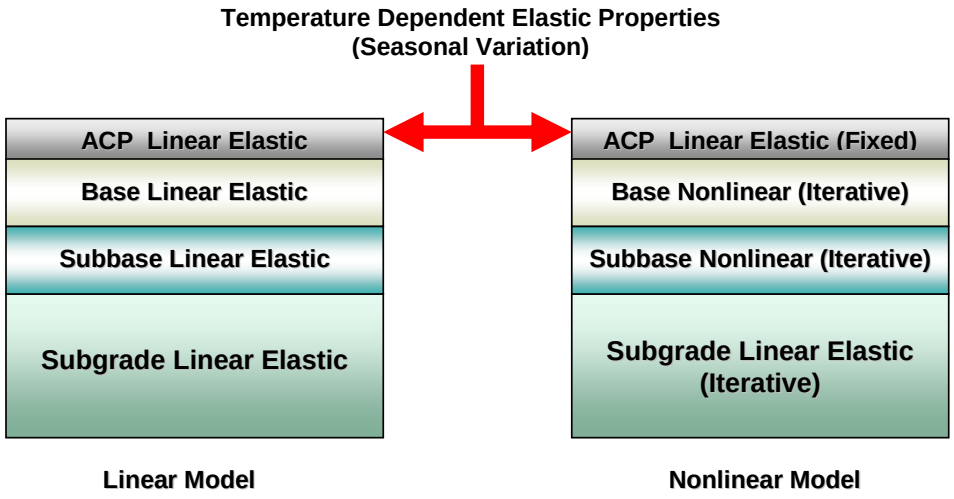

Figure 4.3 – Pavement structure layers subjected to linear and nonlinear analysis.

The discrimination of elements permitted the assemblage of two global stiffness matrices, one of them subjected to the iterative process while the other remained fixed. Since the mesh refines as it gets close to the surface, a considerable amount of elements, which happen to lie on the asphalt layer, are excluded from the iterative process, thus reducing the computation time. At

the end of the analysis, both global stiffness matrices are integrated into a single one, as shown in Equation 4.10.

$$[GK] = [GK]_{fixed\ (ACP)} + [GK]_{iterated\ (Base+Subgrade)} \tag{4.10}$$

After obtaining the total static deflection for each layer under a user defined load, the program determines rutting based on a constitutive model based on the total elastic strain within a pavement layer shown in Equation 2.2.

4.7 Sample case of linear and nonlinear modeling

Table 4.3 presents properties of a sample pavement structure used to compare with the different type of models. The models taken into consideration are the ones described in the previous chapter: a linear model that considers all materials in the pavement structure with a linear elastic behavior; and, a nonlinear model that considers pavement materials to be subjected to an iterative process that obtains both confining pressure and deviatoric stress and implements the constitutive model shown in Equation 4.2, with the exception of the asphalt concrete layer which remains linear elastic. Results of such analyses are graphed on Figure 4.4 for a 9 kips (40 KN) single axle, with 114-psi tire pressure. Similar loading conditions result in similar results for rutting on the four available cases, both two- and three-dimensional linear and nonlinear analyses. Furthermore, the rutting obtained from the 2D FE linear analysis compares well with the ones obtained through VESYS 5, as shown in Figure 4.5 for a single axle load.

Table 4.3 - Sample material parameters for asphalt concrete, base and subgrade layers.

Layer	Thickness (in)	Modulus (ksi)	Material Properties			
			α	μ	k_2	k_3
ACP	3	500.0	0.78	0.35		
Base	12	50.0	0.87	0.25	0.20	-0.20
Subgrade	40	8.0	0.90	0.28	0.20	-0.05

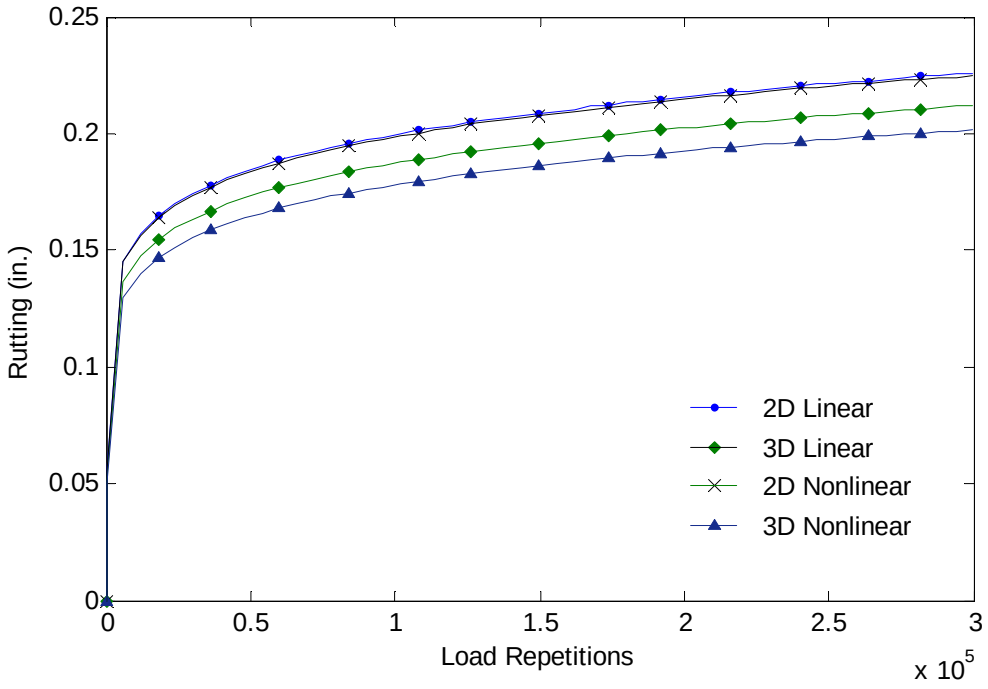

Figure 4.4 – Sample pavement structure results for different models: 2 and 3-D models for both linear elastic analysis and nonlinear analysis using Equation 3.1 constitutive model.

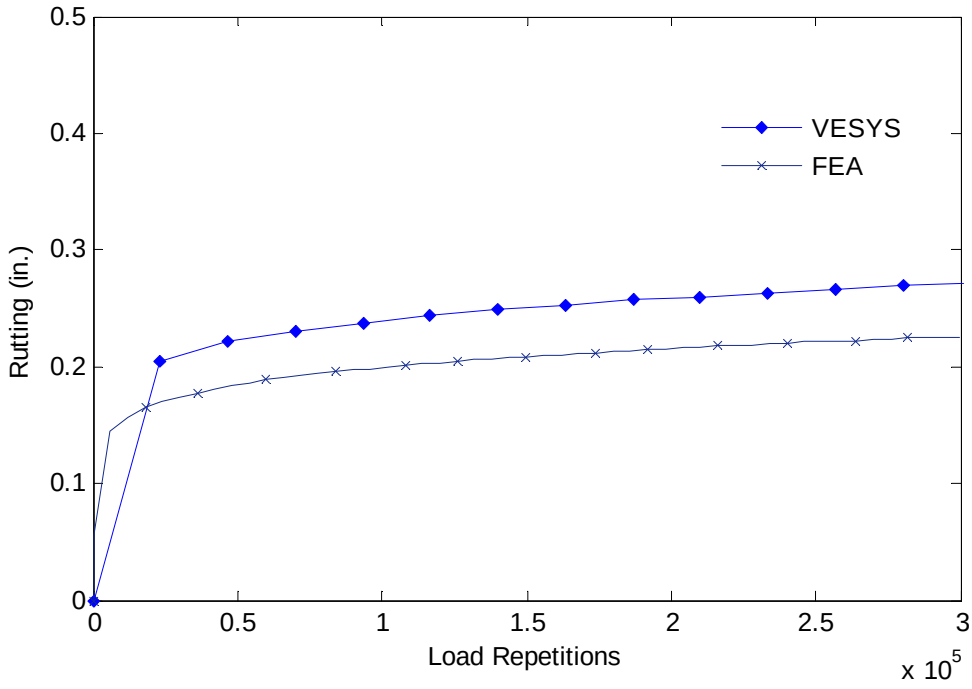

Figure 4.5 - Rutting comparison VESYS vs. FEA 2D linear for a similar pavement structure.

4.8 Finite element modeling of wave propagation systems

Wave propagation problems present general closed-form solutions that are available only for cases with simple boundary conditions, otherwise they contain transcendental functions and infinite roots, resulting in mode jumping, and as a consequence, they require alternate solutions such as finite element or finite difference solutions. The finite element method for wave propagation in multilayered media was developed and generalized by Lysmer (1970), Lysmer and Drake (1972) and Zienkiewicz (1977). Lysmer's method assumes all displacements vary linearly with depth within each layer and the thickness of each layer should be small compared to the wavelength of the shear waves in the layers (Lysmer and Waas 1972).

On the other hand, great effort has been aimed to develop tools for pavement damage assessment implementing finite element modeling to evaluate the surface wave analysis. Ganji

et al. (1997) studied the ability of the SASW test to detect underground obstacles. They also simulated SASW using the finite element method, making use of two computer programs, ANSYS and ABAQUS, to obtain the numerical solution of the surface response of a layered half-space and a pavement system. They assumed wave propagation to occur along the vertical plane with no lateral reflected waves, and used an axisymmetric model with an origin at the impact source. Unlike the static analyses used for predicting the static responses in other studies, the analysis consisted of implicit time integration of the equation of motion. Advantages of the implicit method are that it is suited to structural dynamics problems; it competes with the modal superposition method, and it may be cheaper were many modes would be needed in the modal analysis. It is unconditionally stable and the size of the time step, Δt, in contrast with the explicit method, is limited only by consideration of the accuracy rather than the numerical stability. Besides, nonlinearity can be accommodated without great trouble.

Cho and Lin (2005) developed a numerical model of spectral analysis of surface waves (SASW) method to find surface wave velocities in a multi-layer cement mortar slab system using GT STRUDL, a general purpose finite element program, by implementing a direct integration analysis using Newmark-β method.

4.9 Dynamic analysis

Dynamic analysis of structural systems is a direct extension of the static analysis; the finite element idealization is extended to a situation that is time dependent. Practical time dependent problems range from transient heat conduction and wave propagation to dynamic behavior of structures.

The equation of motion governing the linear dynamic response of the pavement system is defined as

$$\mathbf{M}\ddot{\mathbf{d}} + \mathbf{C}\dot{\mathbf{d}} + \mathbf{K}\mathbf{d} = \mathbf{F} \tag{4.11}$$

where **M** is the mass matrix, **C** is the damping matrix, **K** is the stiffness matrix, **F** is the external load vector acting at the nodal points, and **d,** $\dot{\mathbf{d}}$, $\ddot{\mathbf{d}}$, are is the vector of nodal displacements, velocity and acceleration, respectively.

Finite element dynamic analyses are generally classified into two distinct categories: implicit algorithms and explicit algorithms (Belytschko 1983). In the former, a matrix system is solved one or more times per step towards the solution, and are generally characterized by unconditional stability (i.e. no time step restriction is engendered by stability considerations). Explicit time integration techniques solve the matrix system without storing a matrix or solving a system of equations and generally require small time steps increments to insure numerical stability; thus, requiring many time steps. The step-size restriction is often more rigorous than required for accuracy; however, the computational cost per step is generally much less for explicit than for implicit time integration schemes, as the solution of a system of equations is avoided.

4.10 Explicit time integration algorithm

Explicit direct integration is best suited to wave propagation problems as computer requirements are low. Cost per time step is small as well as the critical time step; thus, these algorithms are not well suited to structural dynamics problems. Both frequencies and modes are not necessary to be computed as compared to implicit methods. Furthermore, nonlinearity can easily be accommodated.

The explicit methods are only conditionally stable. The stability limit is approximately equal to the time for elastic waves to transverse the smallest element. The explicit central difference method is an explicit second order method for approximating the solution of the second order differential equation $y''(x) = f(x, y)$ with initial conditions $y(x_0) = y_0$ and $y'(x_0) = y_0'$ (Cook *et al*. 2001).

With Δt the time step, velocity and acceleration at time step i are approximated by these conventional central difference equations (Bathe and Wilson 1976; Cook *et al*. 2001):

$$\dot{x}_{i+1} = \frac{1}{2\Delta t} \cdot \left(x_{i+1} - x_{i-1} \right), \tag{4.12-a}$$

or

$$x_{i+1} = x_{i-1} - 2\Delta t \cdot \dot{x}_i, \tag{4.12-b}$$

and

$$\ddot{x}_{i+1} = \frac{1}{\Delta t^2} \left(x_{i+1} - 2x_i + x_{i-1} \right). \tag{4.13}$$

These equations are derived from Taylor series expansions of x_{i+1} and x_{i-1} about time $i\Delta t$:

$$x_{i+1} = x_i + \Delta t \cdot \dot{x}_i + \frac{\Delta t^2}{2} \cdot \ddot{x}_i + \frac{\Delta t^3}{6} \cdot \dddot{x}_i + \ldots, \text{ and} \tag{4.14-a}$$

$$x_{i-1} = x_i - \Delta t \cdot \dot{x}_i + \frac{\Delta t^2}{2} \cdot \ddot{x}_i - \frac{\Delta t^3}{6} \cdot \dddot{x}_i + \ldots, \tag{4.14-b}$$

when subtracting the latter from the former equation yields Equation 4.12-a, whereas the addition of them yields Equation 4.12-b. Thus, truncating Equation 4.14-b those terms higher than the second order, the displacement i-1 is obtained as follows:

$$x_{i-1} = x_1 - \Delta t \cdot \dot{x}_1 + \frac{\Delta t^2}{2} \cdot \ddot{x}_1. \tag{4.15}$$

Adequate accuracy is likely to be provided by a small Δt for computational stability. Substituting Equations 4.12-a and 4.13 into 4.11, the following relation is obtained

$$\left(\frac{1}{\Delta t^2}\mathbf{M}+\frac{1}{2\Delta t}\mathbf{C}\right)\mathbf{d}_{i+1}=\mathbf{F}_i-\left(\mathbf{K}-\frac{1}{2\Delta t^2}\mathbf{M}\right)\mathbf{d}_i-\left(\frac{1}{\Delta t^2}\mathbf{M}-\frac{1}{2\Delta t}\mathbf{C}\right)\mathbf{d}_{i-1}. \tag{4.16}$$

4.11 Explicit integration implementation

Implementation of the central difference method into the finite element analysis is conducted by optimization of the code. One of the important techniques for the software implementation is to use a diagonally lumped mass matrix so that the calculation of nodal acceleration is simply a division without inverting the mass matrix, and the linearization is straightforward. For both dynamic and static analyses, the elastic stiffness matrix is the same; however, the mass of the structure is lumped at the nodes.

Assuming that the system has no physical damping, which greatly reduces matrix manipulation, and defining the effective stiffness matrix $\mathbf{K}_{\text{eff}}$ as

$$\mathbf{K}_{eff}=\frac{1}{\Delta t^2}\cdot\mathbf{M}, \tag{4.17}$$

allows Equation 4.8 to be reduced to

$$\mathbf{K}_{eff}\mathbf{d}_{i+1}=\mathbf{F}_i-\left(\mathbf{K}-\frac{1}{2\Delta t^2}\mathbf{M}\right)\mathbf{d}_i-\mathbf{K}_{eff}\mathbf{d}_{i-1}. \tag{4.18}$$

If the equivalent force is defined as

$$\mathbf{F}_{eq}=\mathbf{K}_{eff}\cdot\mathbf{d}_{i+1}, \tag{4.19}$$

then, for each time step, Equation 4.18 can be defined as

$$\mathbf{F}_{eq}=\mathbf{F}_{i+1}-\left(\mathbf{K}-\frac{2}{\Delta t^2}\mathbf{M}\right)\cdot\mathbf{d}_i-\mathbf{K}_{eff}\cdot\mathbf{d}_{i-1}. \tag{4.20}$$

Thus, displacement, acceleration and velocity are calculated at time step $i + 1$ as

$$\mathbf{d}_{i+1} = \mathbf{F}_{eq} \cdot \mathbf{K}_{eff}^{-1}, \tag{4.21}$$

$$\ddot{\mathbf{d}}_{i+1} = \frac{\mathbf{d}_{i+1} - 2\mathbf{d}_i + \mathbf{d}_{i-1}}{\Delta t^2}, \text{ and} \tag{4.22}$$

$$\dot{\mathbf{d}}_{i+1} = \frac{\mathbf{d}_{i+1} - \mathbf{d}_{i-1}}{2\Delta t}, \tag{4.23}$$

respectively. This process is summarized in Figure 4.6.

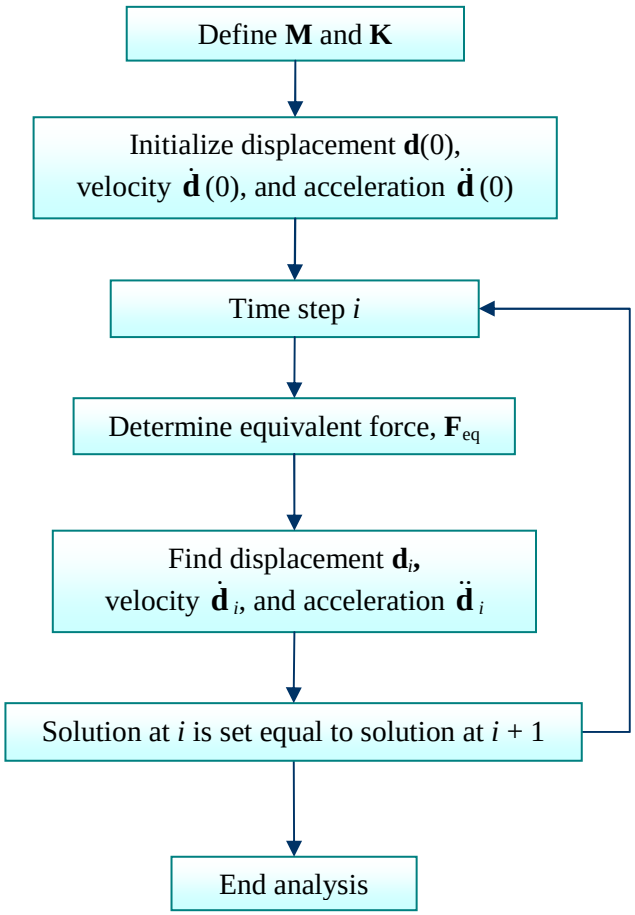

Figure 4.6 – Explicit time integration method.

Since no stiffness and mass matrices of the complete element assemblage need to be calculated, the solution can be carried out on the element level and relatively little storage is required.

The stiffness matrix for an axisymmetric finite element analysis is calculated using Eq. 4.3, where the strain-displacement matrix, **B**, and the elasticity matrix, **D**, are calculated using Eq. 4.4 and Eq. 4.5, respectively. However, the shape functions implemented are the ones corresponding to the quadrilateral linear elements, shown in Table 4.4.

Table 4.4 – Interpolation functions for linear quadrilateral elements (after Zienkiewicz, 1977).

Linear quadrilateral	Shape functions
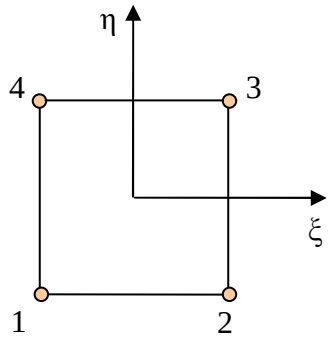	$N^1 = 0.25 \times (1 - \xi)(1 - \eta)$ $N^2 = 0.25 \times (1 + \xi)(1 - \eta)$ $N^3 = 0.25 \times (1 + \xi)(1 + \eta)$ $N^4 = 0.25 \times (1 - \xi)(1 + \eta)$

Implementation of this algorithm into IntPave was compared to Wave2000®, a stand-alone software package for computational ultrasonics which solves the 2D acoustic (elastic) wave equation based on a method of finite differences (CyberLogic, Inc. 1999). Figure 4.7 presents the response for a 4 m wide × 8 m deep section subjected to a 5-cycle modulated 1-kHz force for both 2-D FE time history response using plane strain analysis and explicit time integration method compared to the response provided by Wave2000. The material's properties are ρ = 2,000 kg/m^3, E = 480 MPa, ν = 0.33, c_l = 596 m/s, and c_t = 300 m/s. From the graph it may be seen that both numerical results were similar.

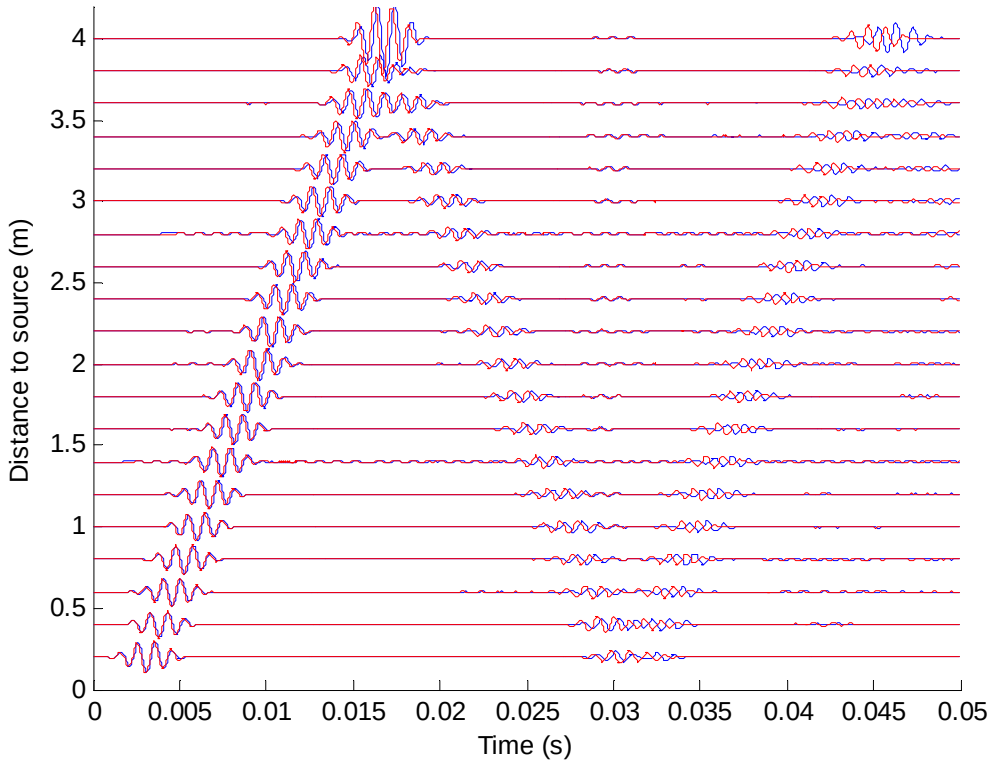

Figure 4.7 - 2-D time history response from FE plane strain analysis with explicit time integration method (blue) compared to Wave2000 (red), for an 8 m wide × 4 m deep section subjected to a 5-cycle 1 kHz force.

Figure 4.8 presents the time histories for the same section subjected to the 5-cycle 1 kHz force but modeled as axisymmetric. Unlike the plane strain, the energy of the finite element analysis diminishes as the wave propagates away from the source as expected due to the spherical propagation of the wave.

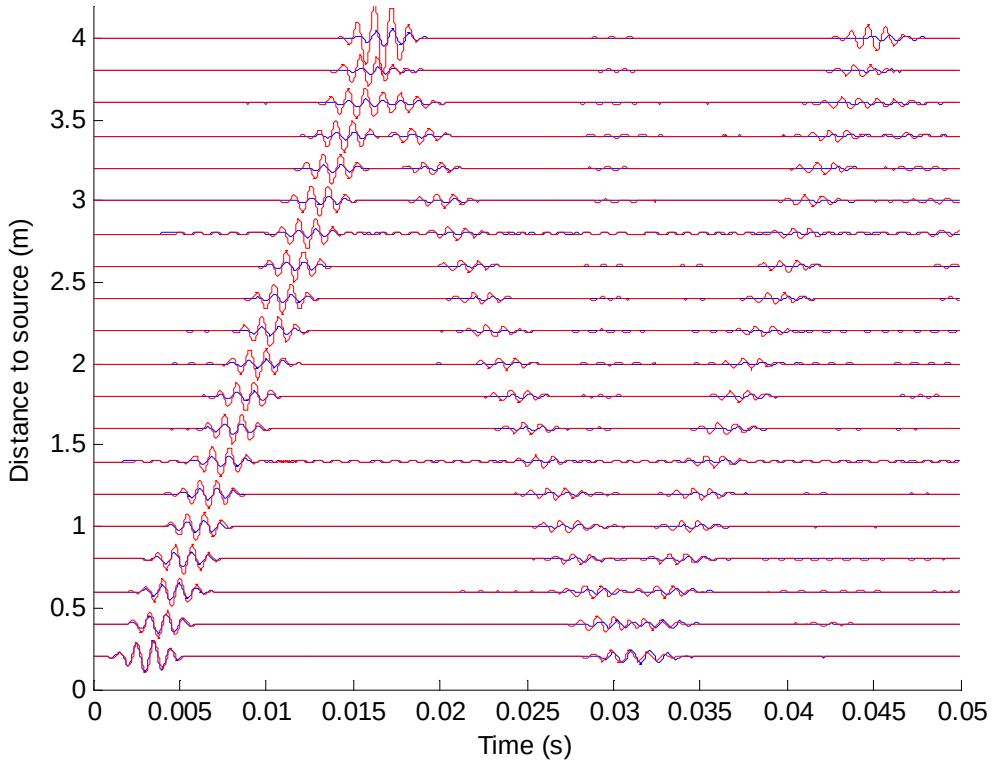

Figure 4.8 - 2-D time history response from FE plane strain analysis with explicit time integration method (blue) compared to Wave2000 (red), for an 8 m wide × 4 m deep section subjected to a 5-cycle 1 kHz force.

In a similar manner, time history responses for an axisymmetric finite element analysis using the implemented explicit time integration method were obtained for a 1.8 m × 1.8 m section subjected to a 200 μs Hamming windowed impulse with properties: ρ = 2,000 kg/m^3, E = 480 MPa, ν = 0.33, c_l = 596 m/s, and c_t = 300 m/s, as shown in Figure 4.9.

4.12 Summary

Implementation of the time integration of the equation of motion into the finite element analysis code of IntPave proved suitable for solving the wave propagation problem. In this

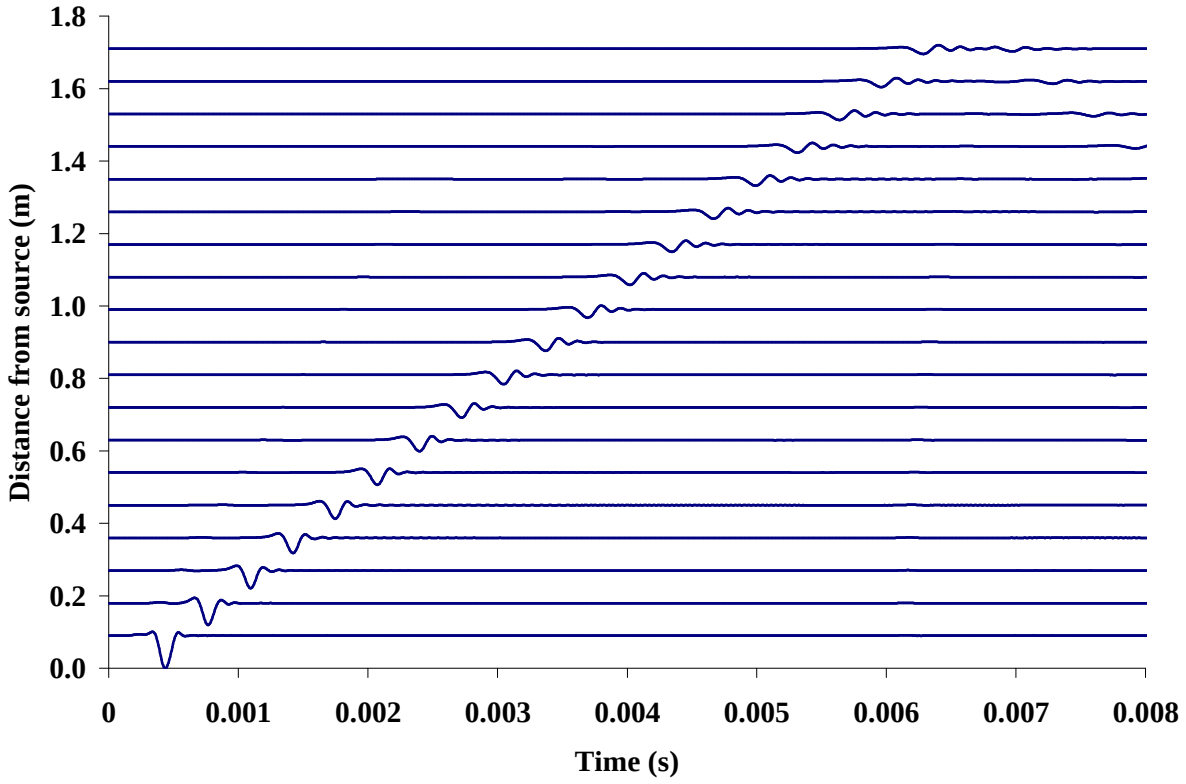

Figure 4.9 - Time history response from FE plane strain analysis with explicit time integration method compared to Wave2000, for an 1.8 m wide × 1.8 m deep section subjected to a 5-cycle 1 kHz force

manner, the numerical results obtained through the finite element method serve as guide to seismic testing techniques. Using the explicit time integration technique greatly reduced the calculation of the dynamic analysis and would easily serve for automating the process to rapidly determine the pavement layers or stiffness profiles in order to assess the pavement performanc. This process can be incorporated into the graphical user interface of IntPave that already includes the analysis of the performance of pavements.

Chapter 5

Damage Factors

5.1 Modeling multiple axle groups

The determination of rutting caused by a truck (as opposed to a single axle) requires an additional procedure to account for the effect and interaction of axle groups. As summarized in Figure 5.1, the first step consists on determining the rut depth generated by a single repetition for the first axle group. To add the contribution to rut of the second axle group, the number of load repetitions of the second axle group to achieve the rut depth already accumulated by the first axle group is backcalculated, and a new rut depth is calculated based on the obtained number of load repetitions plus one. The process repeats until all axle groups are considered, obtaining a final rut depth for a single pass of the entire truck, from which the final deformation is backcalculated. From this deformation, rutting can be obtained for any number of truck passes.

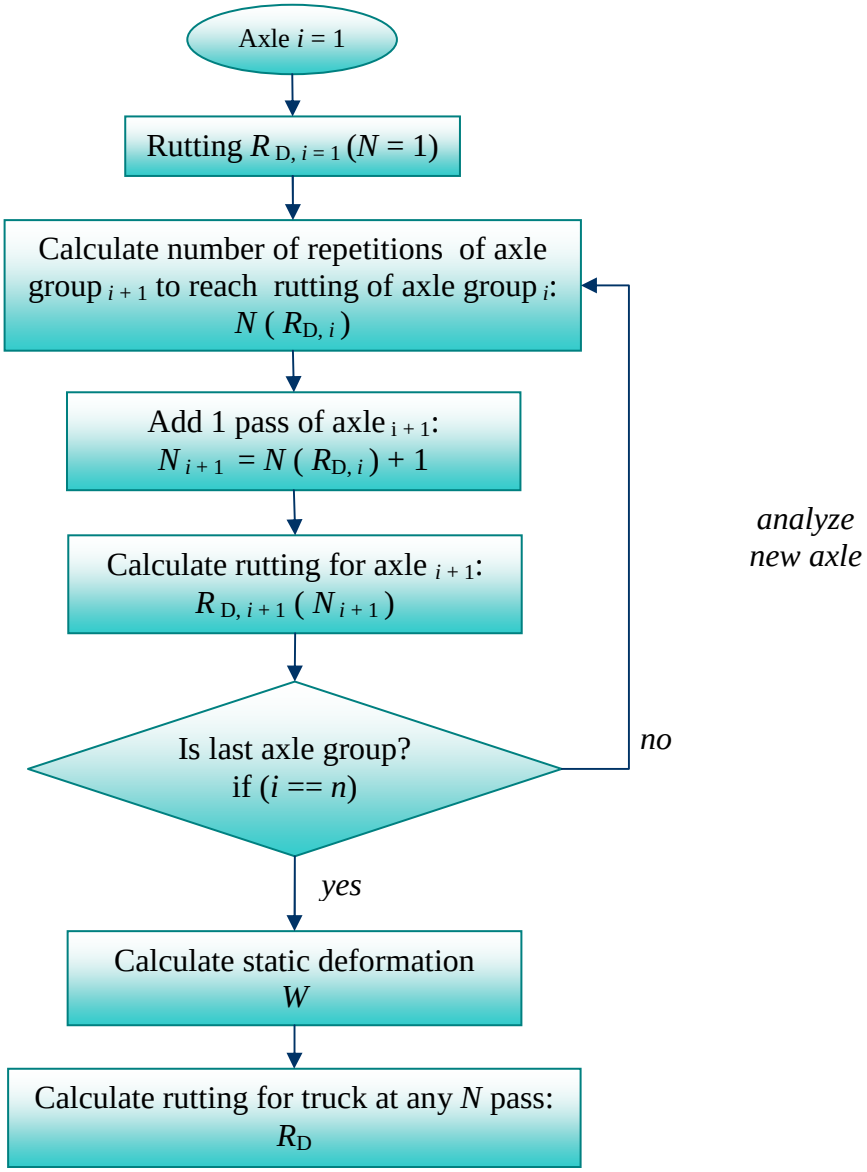

Figure 5.1 - Calculation process of permanent deformation for trucks.

5.2 Seasonal analysis on primary response

Pavements are subjected to different climatic conditions, for that reason, it was necessary to develop the program to perform an analysis that considers seasonal changes on the pavement structure material properties caused by temperature and moisture effects. To avoid reassembling

global stiffness matrices for the asphalt material after every season, the previous assembled stiffness matrix was multiplied by the ratio of modulus of elasticity of the following to the previous season, resulting in less computation time.

5.3 Case study

Variation in material properties with respect to time (due to temperature variation) can be simplified into five seasons, as shown in Table 5.1. These parameters shown for the asphalt concrete layer were obtained from US281 near Jacksboro, TX (Zhou and Scullion 2002). Typical cross-section of the site consists of an 8-in. (203 mm) asphalt concrete layer, a 15-in. (381 mm) base layer on top of subgrade. The effect of seasonal changes on rutting is evident as shown in Figure 5.2 where it is evident that rate of rutting is greater at higher temperatures.

Table 5.1 - Sample seasonal variation for asphalt concrete layer.

Season	Temp (°F)	Modulus (ksi)	α	μ
1	89	211	0.610	0.260
2	84	243	0.638	0.263
3	92	194	0.598	0.250
4	95	180	0.568	0.245
5	91	200	0.598	0.259

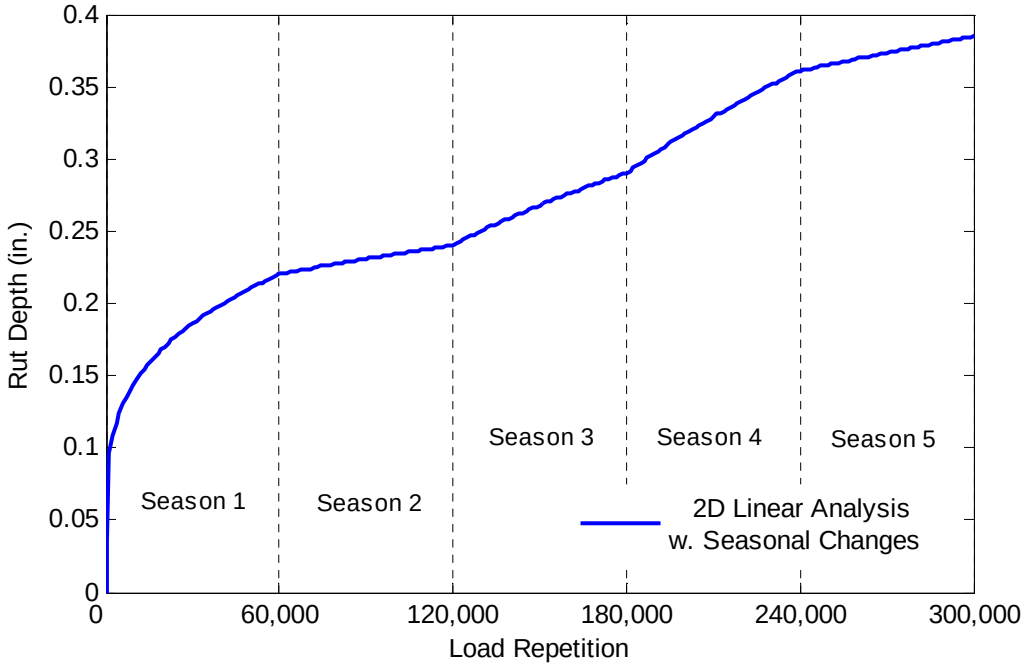

Figure 5.2 - Seasonal variation effects on rut depth.

5.4 Damage factors based on AASHTO

Pavements are designed to allow an anticipated number of axle repetitions of a particular magnitude given an expected service life. Design methods typically express the damage caused by mixed traffic loads in terms of a base reference axle load, namely the 80-KN (18-kip) equivalent single-axle load (ESAL). Damage caused by one pass of a vehicle or an axle group over a pavement can be described by the number of ESALs necessary to have the same pavement life. If a different axle loading is present, an equivalent axle load factor (EALF) is obtained to convert different axle load repetitions into the equivalent standard axle load repetitions. This value depends on the type of pavements, thickness or structural capacity and the terminal conditions at which the pavement is considered failed. These load equivalency factors (LEFs)

for both flexible and rigid pavements are tabulated in the AASHTO Guide for Design of Pavement Structures (AASHTO 1993).

The following regression equations describe the process for determining the equivalent axle load factor for flexible pavements,

$$\log\left(\frac{1}{EALF}\right)=\log\left(\frac{W_{tx}}{W_{t18}}\right)=4.79\log(18+1)-4.79\log\left(L_x+L_2\right)+4.33\log L_2+\frac{G_t}{\beta_x}-\frac{G_t}{\beta_{18}} \quad (4.14)$$

$$G_t=\log\left(\frac{4.2-p_t}{4.2-1.5}\right), \quad (4.15)$$

$$\beta_x=0.40+\frac{0.081\left(L_x+L_2\right)^{3.23}}{\left(SN+1\right)^{5.19}L_2^{3.23}}, \quad (4.16)$$

where W_{tx} is the number of x-axle load applications, W_{t18} is the number of 18-kip single-axle load applications, L_x is the load in kip on one single axle, one set of tandem or tridem axles; L_2 is the axle code (1 for single axle, 2 for tandem axles, and 3 for tridem axles); SN is the structural number; p_t is the terminal serviceability; G_t is a function of p_t as shown in Equation 4.15; and β_{18} is the value of β_x when L_x is equal to 18 and L_2 is equal to 1 (Huang 2004).

The equivalent axle load factor is calculated for each single axle group. However, both formulations do not take into consideration when an axle group is larger than a tridem axle. When an axle group consists of four axles or more, the EALF is obtained for sets of tridem axles adding to the number the one corresponding to an extra EALF calculated for either a single or tandem axle, until all axles are totaled. Besides considering the number of axles within an axle group for determining the equivalent axle load factor, the axle spacing is also taken into consideration. The equivalent load factors are calculated for a standard axle spacing of 48 in. On the other hand, if the axle spacing exceeds 72 in. then the EALF for that given axle must be calculated as a single axle. Whenever the axle spacing is within 48 in. and 72 in. then the EALF

must be calculated for these two distances, and finally an intermediate value must be obtained by linearly interpolated from these values. In order to compute the load factor for a truck, then all axles' EALFs must be added together. If a damage factor is desired from a comparative analysis, then a ratio of EALFs is obtained from a case truck by a standard truck and multiplied by a ratio of carrying cargos of each truck.

Load equivalency factor for a vehicle consisting of *n* axles is obtained as the sum of load equivalent factors for all i axles, as shown in Equation 5.1.

$$LEF_{\text{Truck}} = \sum_{i=1}^{n} LEF_i \,. \tag{5.1}$$

In order to establish a comparison between two vehicles, damage could be normalized to a reference vehicle. It is possible to make use of these AASHTO factors to establish damage factors based on the comparison of two vehicles based on a ratio of equivalent single-axle loads per vehicle, setting one of the trucks as the reference vehicle. Usually, a 356 kN (80 kip) T2S2 standard truck is set as reference vehicle. Thus, this damage factor is a multiplier for converting the number of vehicles with distinctive axle configurations and axle loading to the number of standard vehicles, usually 356 kN (80 kip) T3S2 trucks.

Another appropriate measure that might be taken into consideration consists on normalizing damage per weight of cargo transported. Thus, a ratio of load equivalency factors is obtained from a heavy truck by a standard truck and multiplied by a ratio of carrying cargos of each truck, as reflected in Equation 5.2,

$$DF = \frac{LEF_{\text{Heavy}}}{LEF_{\text{Standard}}} \cdot \frac{Payload_{\text{Standard}}}{Payload_{\text{Heavy}}}, \tag{5.2}$$

to account for the number of trips necessary to carry the same amount of cargo, hence compensating the heavier truck for requiring less repetitions than the lighter truck.

5.5 Damage factors based on distress models

The traditional equivalency approach based on AASHTO's load equivalency factors has limitations when evaluating damage as they fail to consider the load characteristics such as number of tires per axle, tire spacing, and complex axle configurations. Moreover, these load equivalency factors are derived from the empirical equations explained in the previous section and, despite being developed to depend on the type of pavement, structural capacity and its terminal condition, they lack a mechanistic basis. As previously described, IntPave has the capability of calculating distresses for trucks, even considering non-standard axle configurations, and, unlike AASHTO, it rather focuses on the damage caused by the tire pressure rather than the axle. Damage factors based on a failure criterion depending on the type of distress using a mechanistic-empirical method may be established to provide a comparative tool similar to damage factors based on AASHTO load equivalency factors. Moreover, a similar criterion can be established to develop these factors based on the pavement service life. Damage factors based on fatigue cracking or rutting can be established on the number of repetitions to reach failure. In the case of fatigue cracking failure would be attained at 20% cracked area in the wheel path, whereas failure in rutting is commonly established at a rut depth of 12.5 mm (0.5 in.). Damage factors based on distress, either rutting or fatigue cracking, for comparing two vehicles are thus defined as shown in Equation 5.3:

$$DF = \frac{N_{d,\,\text{Standard}}}{N_{d,\,\text{Heavy}}} \cdot \frac{Payload_{\text{Standard}}}{Payload_{\text{Heavy}}}, \tag{5.3}$$

where N_d is the total number of truck repetitions or passes to produce failure in the given type of distress. The damage factor *DF* is compensated by the payload ratio to account for the number of trips required by each truck to carry a similar amount of cargo.

5.6 Case study

This study aims to address the effects of heavy trucks on pavement rutting as compared to standard trucks. Two case studies are shown for this purpose. Determination of damage factors requires the consideration of typical highway cross-sections and gross loads of interest. When defining the trucks for each load category, appropriate truck axle configurations were assigned to each load group to fulfill the requirements of overweight permit policies in most highway agencies. Typical highways cross-sections were defined for the Interstate Highways, U.S. Highways, State Highways and Farm to Market Roads, as shown in Table 5.2.

Table 5.2 - Typical highway pavements structural properties and cross-sectional thicknesses.

Pavement Type	ACP		Base		Subgrade
	Thickness	E	Thickness	E	E
Interstate Highway	254 mm (10 in.)	3,450 MPa (500 ksi)	305 mm (12 in.)	345 MPa (50 ksi)	69 MPa (10 ksi)
U.S. Highway	152 mm (6 in.)	3,450 MPa (500 ksi)	305 mm (12 in.)	345 MPa (50 ksi)	69 MPa (10 ksi)
State Highway	76 mm (3 in.)	3,450 MPa (500 ksi)	305 mm (12 in.)	207 MPa (30 ksi)	69 MPa (10 ksi)
Farm to Market Road	25 mm (1 in.)	2,070 MPa (300 ksi)	254 mm (10 in.)	207 MPa (30 ksi)	69 MPa (10 ksi)

5.6.1 Scenario 1 – Same gross vehicle weight with different axle configurations

Table 5.3 presents axle load configurations of six different trucks that will be compared to a standard 355 kN (80 kip) T3S2 truck. All trucks have a gross vehicle weight (GVW) of 520 kN (117 kips), about 46% heavier than standard load. Trucks 1 and 2 have similar axle configuration, i.e. two tridem axles, whereas the remaining trucks consist of a tandem and a

Table 5.3 - Truck configurations for defined gross loads of interest.

Truck	**Standard T3S2**	**Case 1 T4S3**	**Case 2 T4S3**	**Case 3 T3S4**	**Case 4 T4S4**	**Case 5 T4S4**	**Case 6 T4S4**
Steering Axle, kN (lbs.)	53 (12)	53 (12)	53 (12)	53 (12)	53 (12)	53 (12)	53 (12)
Rear Tractor Axle, kN (kips)	151 (34)	233 (52.5)	209 (47)	213 (48)	187 (42)	160 (36)	187 (42)
Trailing Axle, kN (kips)	151 (34)	233 (52.5)	258 (58)	253 (57)	280 (63)	307 (69)	280 (63)
Trailing Axle Type	Tandem	Tridem	Tridem	Tridem	Quadrum	Quadrum	Quadrum
Axle Spacing	1.22 m (48 in.)	1.22 m (48 in.)	1.22 m (48 in.)	1.22 m (48 in.)	1.22 m (48 in.)	1.22 m (48 in.)	1.37 m (54 in.)
Truck Configuration	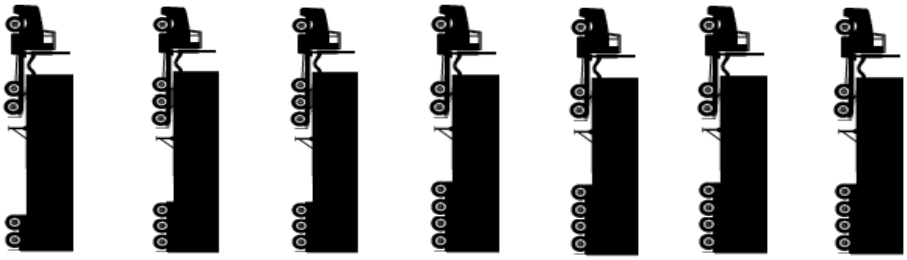						
Gross Vehicle Weight, kN (kips)	355 (80)			520 (117)			
Empty Vehicle Weight, kN (kips)	147 (33)			198 (44.5)			
Payload, kN (kips)	209 (47)			322 (72.5)			

quadrum axle. The difference lies on how loading is distributed onto these axles. Furthermore, the impact of axle spacing is evaluated on Trucks 4 and 6, which differ only on their axle spacing, maintaining identical axle loading and configuration.

Almost all highway agencies use the AASHTO load equivalency factors to compare damage relative to standard T3S2 356 kN (80 kip) trucks. Table 5.4(a) presents the AASHTO

damage factors obtained for a typical U.S. Highway pavement structure (as defined in Table 5.2) at the GVW's defined in Table 5.3. Case 3 where the rear tractor axle is heavily loaded provides the highest damage factor, while Cases 1 and 2 where the load on the rear tractor axle is distributed on three axles yield the lowest damage factors. Considering the payload hauled for each trip, Cases 2 and 3 result in less damage to the pavement as compared to the standard truck.

Table 5.4 - Damage factors obtained from AASHTO method and IntPave for a typical U.S. Highway pavement structure.

a) AASHTO Method

Truck	**Standard T3S2**	**Case 1 T4S3**	**Case 2 T4S3**	**Case 3 T4S4**	**Case 4 T4S4**	**Case 5 T4S4**	**Case 6 T4S4**
Load equivalency factor (LEF)	2.38	3.15	3.33	5.38	4.25	3.81	4.74
Damage factors without payload	1.00	1.33	1.40	2.26	1.79	1.60	1.99
Damage factors with payload	1.00	0.86	0.91	1.47	1.16	1.04	1.29

b) Using IntPave

Truck	**Standard T3S2**	**Case 1 T4S3**	**Case 2 T4S3**	**Case 3 T4S4**	**Case 4 T4S4**	**Case 5 T4S4**	**Case 6 T4S4**
Damage factors without payload	1.00	1.80	2.19	4.71	2.41	1.58	1.79
Damage factors with payload	1.00	1.17	1.42	3.06	1.56	1.02	1.16

Damage factors from IntPave are shown in Table 5.4(b) for a terminal rutting of 12.5 mm (0.5 in.). Similar to the AASHTO procedure, the greatest damage factor corresponds to Case 3. However, the smallest damage factor is obtained for Case 5 as opposed to Case 1 from the AASHTO process. This perhaps occurs because the AASHTO procedure does not consider the interaction of the different tires in an axle group. This observation is supported by comparing Cases 4 and 6 where the only difference is the spacing between axles within the axle group. In

the AASHTO methods the damage factors from Cases 4 and 6 are fairly close, with Case 6 (with farther axle spacing) yielding a higher damage factor. The results from IntPave demonstrate a different trend, when the axles are placed closer (Case 4) the damage factor is greater than Case 6. This trend is more intuitive since the interaction between the axles is more significant as they become closer to one another.

The damage factors considering the hauling of the payload from the two methods are compared in Figure 5.3. The damage factors from the rutting criteria of IntPave are significantly greater than the ones from AASHTO in almost all cases.

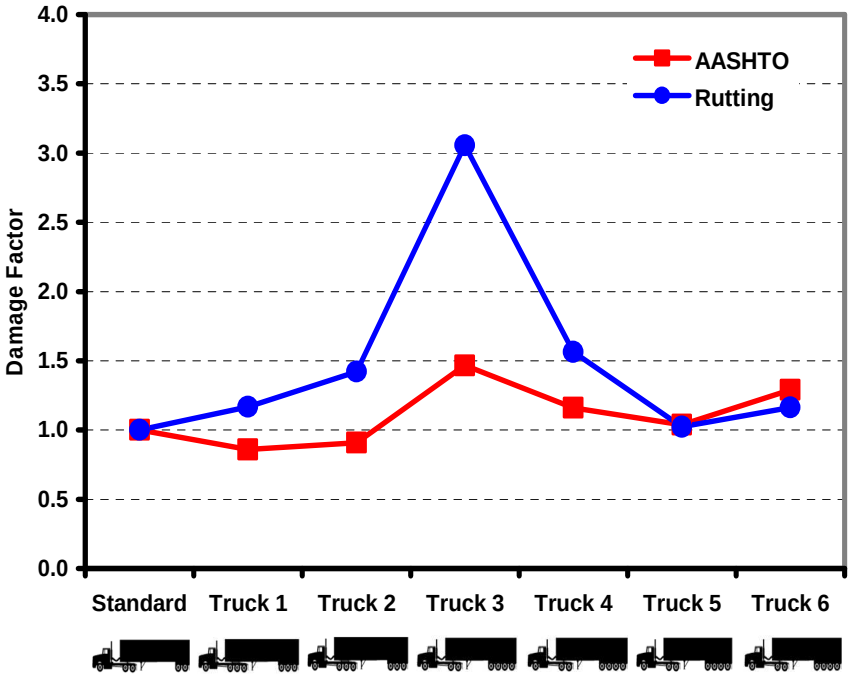

Figure 5.3 - Damage factors based on AASHTO and rutting for a typical U.S. Highway pavement structure.

To match the results from the two methods, the terminal rut depth in IntPave was varied. As shown in Figure 5.4, as the terminal rutting is changed from 6 mm (0.25 in.) to 25 mm (1 in.), the damage factors in rutting dramatically decreases. Comparing the AASHTO damage factor,

terminal rut depths of greater than 25 mm (1 in.) has to be assumed to obtain similar results between the two methods. These results clearly exhibit that the damage factors depend on failure criteria, and axle loading and configuration.

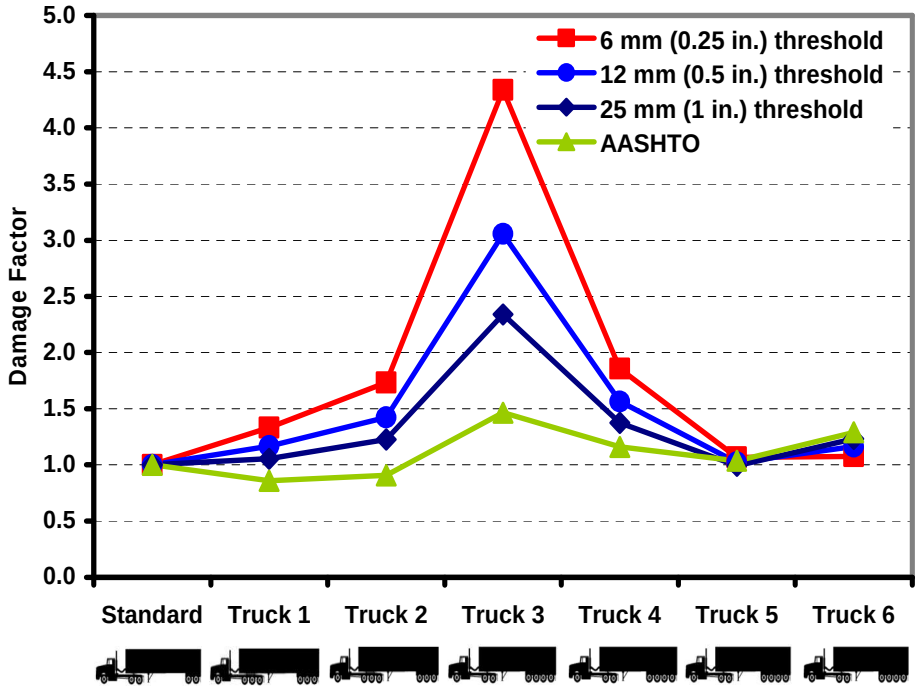

Figure 5.4 - Damage factors based on AASHTO method and on the ratio of truck passes to reach failure criterion for rutting for a typical U.S. Highway pavement structure considering payload.

5.6.2 Scenario 2 – Analysis of heavy payloads

The second case scenario takes into consideration heavy trucks. Axle configuration and loading for four different trucks are shown in Table 5.5. Once again, the damage factors from these trucks were compared to a standard 355 kN (80 kip) T3S2 truck. GVW increments of 178 kN (40 kips) were considered starting from the standard 355 kN (80 kip) truck until a GVW of 1,068 kN (240 kip) is reached. For each GVW, the axle configuration was changed until they

Table 5.5 - Truck configurations for defined gross loads of interest.

Truck	**Standard T3S2**	**Case 1 534 kN (120-k)**	**Case 2 712 kN (160-k)**	**Case 3 890 kN (200-k)**	**Case 4 1,068 kN (240-k)**
Steering Axle, kN (lbs.)	53 (12)	53 (12)	53 (12)	53 (12)	53 (12)
Rear Tractor Axle, kN (lbs.)	151 (34)	169 (38)	160 (36)	169 (38)	160 (36)
Trailing Axle, kN (lbs.)	151 (34)	311 (70)	498 (112)	667 (150)	854 (192)
Trailing Axle Type	Tandem	Quadrum	Trunnion	Trunnion	Trunnion
Truck Configuration					
Gross Vehicle Weight, kN (lbs.)	355 (80)	534 (120)	712 (160)	890 (200)	1,068 (240)
Empty Vehicle Weight, kN (lbs.)	147 (33)	165 (37)	165 (37)	182 (41)	200 (45)
Payload, kN (lbs.)	209 (47)	369 (83)	547 (123)	707 (159)	867 (195)
Payload ratio	1.00	1.77	2.62	3.38	4.15

exerted “legal” loads according to Texas regulations. In order to have the trucks “legal”, appropriate truck axle configurations were assigned to each load group to fulfill the requirements of Texas Oversize/Overweight Permit Rules and Regulations. In that regulation, the maximum axle weight limits for an axle or axle group are based on the lesser of a 115 kN/m (650 lb/in.) of tire width or a maximum load of 110 kN (25 kip) for a single axle, 200 kN (46 kip) for a two axle group, 270 kN (60 kip) for a three axle group, 310 kN (70 kip) for a four axle group, and 270 kN (60 kip) for trunnion configuration with a total of 16 tires per two axles (TxDOT 2007b).

As shown in Table 5.6, damage factors increase as the GVW increases. Nonetheless, if rutting criterion is taken into consideration different trends become evident for the two heaviest trucks, as shown in Figure 5.5, as their damage factors decrease compared to the Case 2 truck, whereas AASHTO considers these trucks similar or slightly more damaging than Case 2. Although the GVW is larger for the two heaviest trucks, the load is distributed over a larger number of tires. This feature is manifested on the damage factors based on the rutting criterion, but not on the AASHTO criterion.

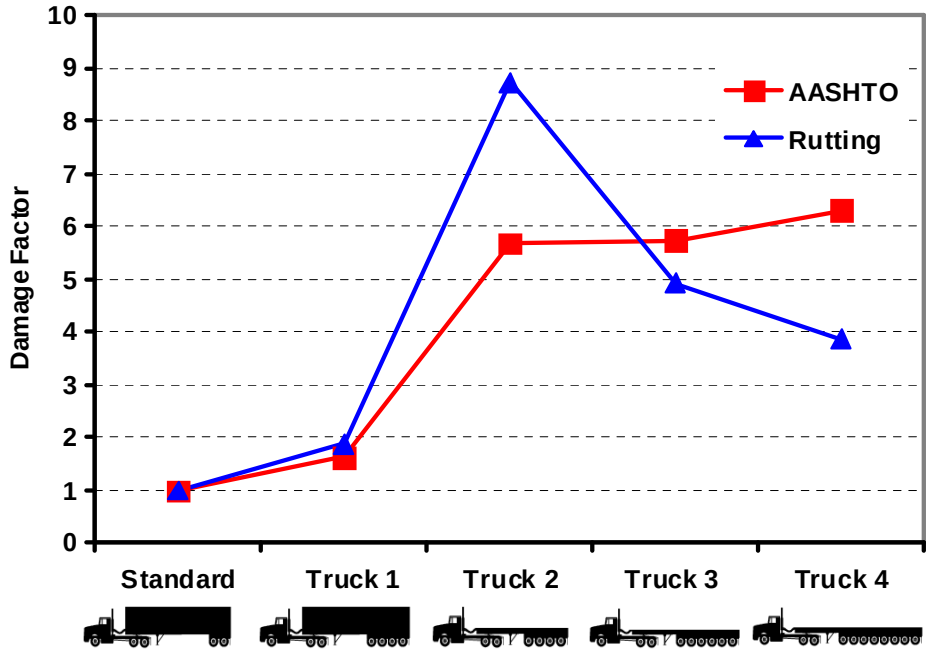

Figure 5.5 - Damage factors based on AASHTO method and on the ratio of truck passes to reach failure criterion for rutting for a typical U.S. Highway pavement structure considering payload.

Table 5.6 - Damage factors obtained from AASHTO's load equivalency factors for an U.S. Highway typical pavement structure.

a) AASHTO

Truck	**Standard T3S2**	**534 kN (120-k)**	**712 kN (160-k)**	**890 kN (200-k)**	**1,068 kN (240-k)**
Load equivalency factor (LEF)	2.38	3.87	13.5	13.6	15.0
Damage factors without payload	1.00	1.63	5.69	5.74	6.31
Damage factors with payload	1.00	0.92	2.17	1.70	1.52

b) Using IntPave

Truck	**Standard T3S2**	**534 kN (120-k)**	**712 kN (160-k)**	**890 kN (200-k)**	**1,068 kN (240-k)**
Damage factors without payload	1.00	1.88	8.72	4.92	3.87
Damage factors with payload	1.00	1.06	3.33	1.46	0.93

Furthermore, according to the AASHTO criteria, Case 1 and Case 2 trucks are considered to have equal axle configurations, even though the former truck has a 311 kN (70 kip) quadrum trailing axle group while the latter has a 498 kN (112 kip) trunnion. As such, it seems that the AASHTO procedure pays attention to axle loading while overlooking the number of tires per axle. Case 1 carries 78 kN (17.5 kip) per axle along the quadrum axle and Case 2 truck carries 125 kN (28 kip) per axle along the trunnion; however, the former carries 120 kN (4.4 kip) per tire while the latter carries 16 kN (3,500 lb) per tire.

Figure 5.6 compares the damage factors obtained for all trucks considering all pavement types whose properties were shown in Table 5.2. For each pavement type the standard 355 kN (80 kip) truck was used as basis for comparing other trucks. The AASHTO method does not have an established methodology for considering groups with more than three axles and, thus, load equivalency factors are appended to get a rough estimate of the total equivalency for the trunnion cases. The trends between the AASHTO method and the mechanistic one developed by IntPave are different, as shown in Figure 5.6 and 5.7, respectively. For the AASHTO method,

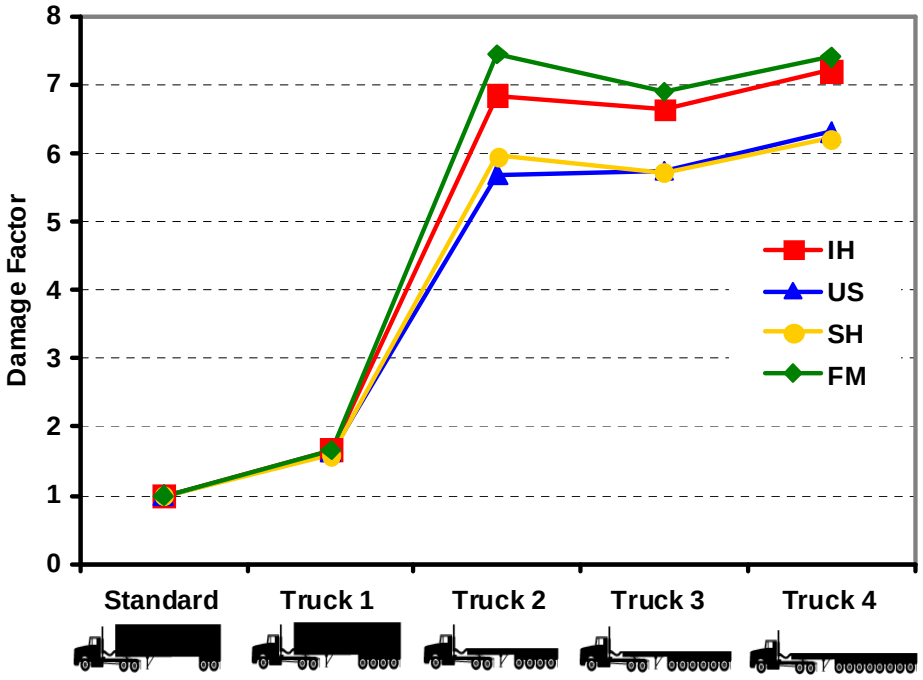

Figure 5.6 - Damage factors based on AASHTO for typical Interstate Highway (IH), U.S. Highway (US), State Highway (SH) and Farm to Market Roads (FM) pavement structures.

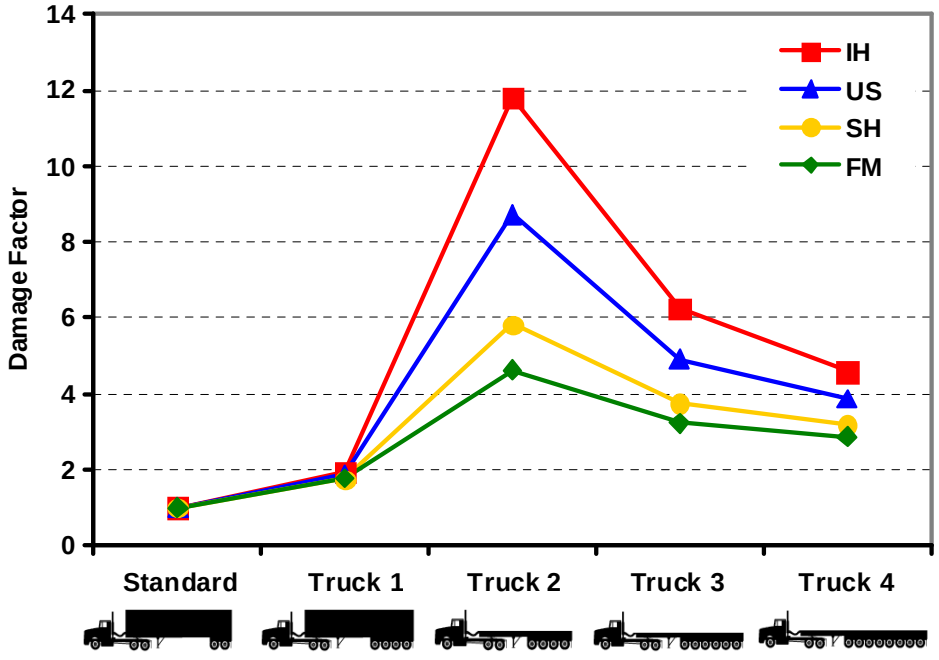

Figure 5.7 - Damage factors based on Mechanistic Approach for typical Interstate Highway (IH), U.S. Highway (US), State Highway (SH) and Farm to Market Roads (FM) pavement structures.

the impact of the pavement structure on the damage factors is rather small and no trend between the type of pavement and the damage factor is evident. However for the mechanistic approach, as the pavement structure becomes more substantial, the damage factor becomes larger. The trends from the mechanistic methods seem more reasonable.

Figure 5.8 presents the damage factors for the mechanistic method when the hauled loads to compensate for the number of trips required to carry a given load is considered. In this case, the damage factors are substantially less, and in some cases the damage factors are less than one, indicating less damage to the pavement relative to the standard truck

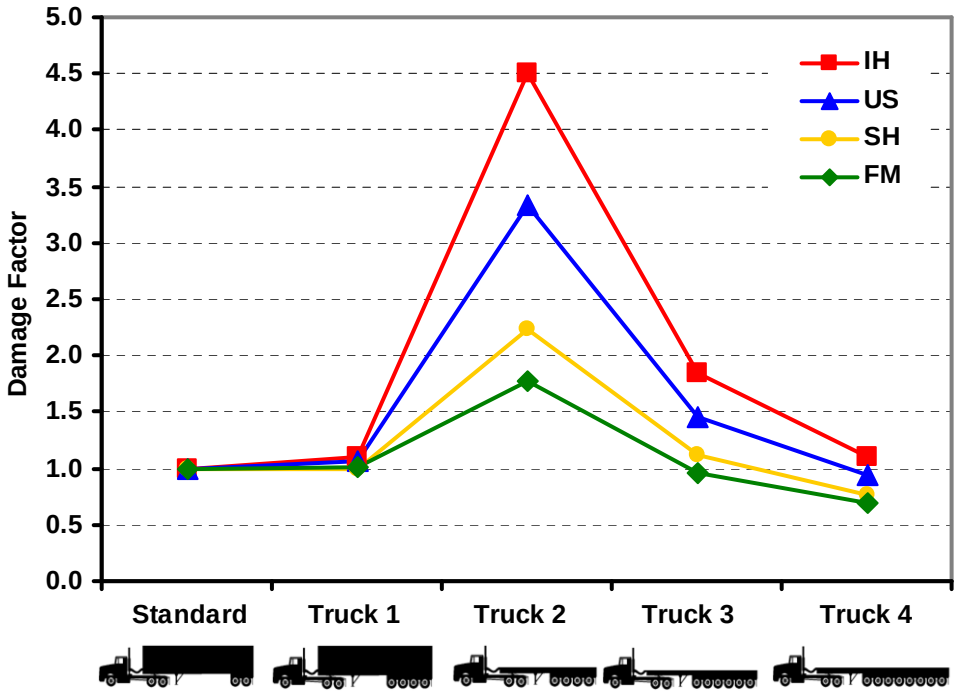

Figure 5.8 - Damage factors based on rutting considering cargo for typical Interstate Highway (IH), U.S. Highway (US), State Highway (SH) and Farm to Market Roads (FM) pavement structures.

5.7 Impact of overload

The impact of overloaded trucks was also evaluated. For this purpose, the GVW's for the trucks defined in Table 5.5 were increased by 20%, thus making the trucks "illegal", as they fail to comply the overweight regulations. As shown in Figure 5.9 for a U.S. Highway pavement type, such overloading has an impact on damage factors. Damage factors based on AASHTO doubled, being consistent with the "fourth power law", while the mechanistic damage factors based on the rutting criterion increased by a factor of 2.7 to 1. AASHTO would tend to underpredict damage when loading exceeds regulations.

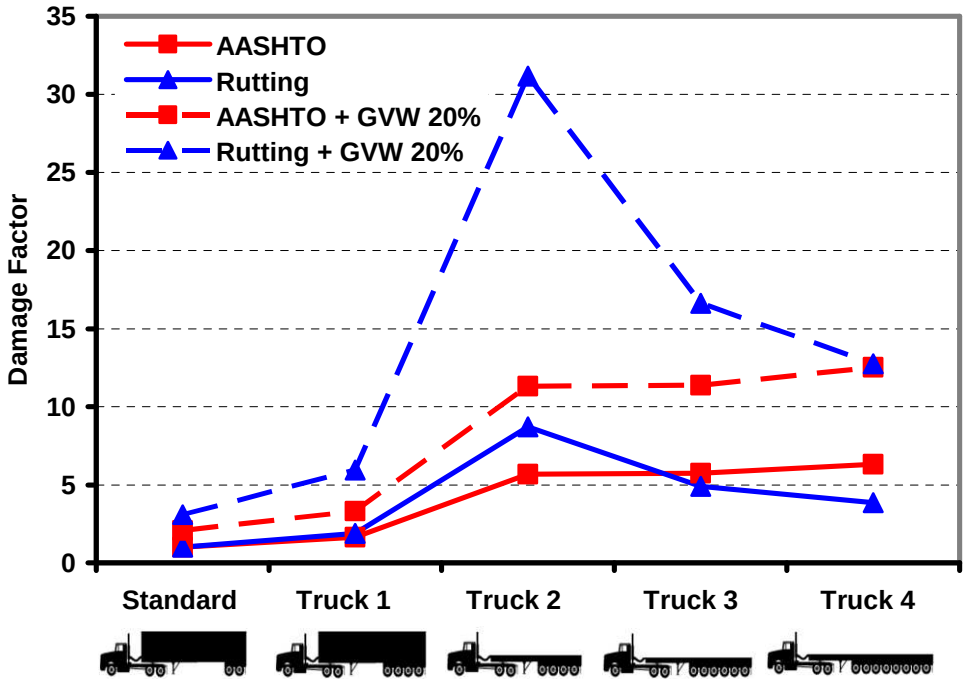

Figure 5.9 - Effect of extra 20% gross vehicle weight on damage factors based on AASHTO approach and rutting for a typical U.S. Highway pavement structure.

5.8 Summary

Different models have been developed over the years to evaluate pavement distresses. Models developed based on the elastic layer theory have proven efficient on estimating distress under daily traffic and different climatic seasons. However, these models fail to consider the impact of truck configuration on damage rigorously. For that reason, the finite element program Integrated Pavement Damage Analyzer (IntPave) was developed for rigorously analyzing distress of pavements. The developed program has the advantage of rapid execution time due to optimizations performed on the programming code. Furthermore, IntPave allows comparing the level of distress caused by a standard and a non-standard truck. Case studies were presented based on typical highway pavements to determine damage factors based on the number of truck passes to reach failure in rutting and compare them to damage factors based on traditional AASHTO load equivalency factors. It was found that the traditional equivalency approach had limitations when evaluating damage as they fail to consider the load characteristics such as number of tires per axle, tire spacing, and complex axle configurations. As a consequence, in some cases these factors tend to be mis-estimated. The study also proved that overloaded vehicles that are not within the overload permit policies do greatly increase pavement deterioration as proven by all approaches for damage equivalencies.

Chapter 6

Permit Cost Estimation for the Movement of Heavy Trucks on Flexible Pavements

6.1 Introduction

A methodology based on a mechanistic-empirical (M-E) analysis was developed for the estimation of permit fees based on the truck axle loading and configuration and the predicted pavement deterioration it causes. This methodology was implemented into IntPave and a parametric study was carried to demonstrate the impact on the cost of the permit fee based on various heavy truck loads and axle configuration, traffic volume and pavement structure.

6.2 Background

Trucking accounts for about 80% of freight transportation in the United States (NRC 2002). At the Federal level, trucks are considered "legal" provided they meet weight guidelines of the 1975 Federal Bridge Formula B; however, vehicles operating on the state and local highway system are not subject to such guideline. Additionally, at least 30 states permit exceptions to the Interstate system axle load limits or gross weight limits either with or without special permits (Sivakumar *et al*. 2007). In Texas, for instance, a gross vehicle weight (GVW) that exceeds 250,000 lb (1,100 kN) is considered "super-heavy load" and requires a permit before traveling on a state-maintained roadway system (Chen *et al*. 1995). These permits are typically requested to transport loads such as transformers, generators, or combustion turbines. Implementation of the North American Free Trade Agreement (NAFTA) among Canada, Mexico, and the US has called the attention of some highway agencies along the borders to

understand the impact of heavier axle loads and new axle configurations on their highway networks. Highways designed to carry vehicle loads of 80 kips (350 kN) could be trafficked with gross vehicle loads of over 120 kips (500 kN), by trucks with different tire and axle configurations. The use of heavy loads and new vehicle configurations has a major impact on the structural and functional performance of the highway network. Hence, highway agencies urgently need tools to predict the additional damage and its economic impact of allowing such trucks to use the highway system.

Accurate predictions of pavement performance and/or distresses are critical to obtain meaningful results from any developed permit fee estimation algorithm. However, the inputs to these algorithms need to be readily available and their computational speed needs to be acceptable. Mechanistic-empirical (M-E) models tend to meet these criteria. In these models, the design procedure calculates pavement responses (e.g., stresses, strains, deflections) and uses those responses to compute incremental damage over time. Then the Mechanistic-Empirical Design Guide empirically relates damage to observed pavement distresses. The outputs from the procedure are pavement distresses and smoothness.

The fact that the highway system accommodates a vast variety of vehicles serving a multiplicity of uses has led to the development of highway cost allocation studies that seek to distribute costs equitably among all vehicle classes. The theoretical foundation of the proposed methodology for assessing super-heavy permit fees stems from the principles of these studies. Highway cost allocation studies (HCASs) have been conducted at the federal and state levels to compare the expenses that various groups of highway users necessitate to provide and maintain the highway infrastructure to the revenues that each group generates.

All federal and most state HCASs use the cost-occasioned approach for the allocation of highway development, maintenance, and operation costs. Under this approach, each user pays the highway costs that it creates. Although the philosophy of this approach appears logical, it is controversial in terms of what costs to consider. The cost-occasioned approach is widely used because it promotes an economically efficient allocation of scarce resources (ECONorthwest 2007). The principal alternative to the cost-occasioned approach is the benefits approach. Under this approach, the greater the benefits, the greater the share of user fees a vehicle class pays, regardless of its contribution to highway costs (Boilé *et al*. 2001). Within the cost occasioned approach, the most common method for allocating costs to different vehicle classes is the incremental method. Under this method, the minimum design (considered adequate for light vehicles only) is considered a common responsibility of all highway users and shared by all vehicle classes based on common measures such as vehicle miles traveled (VMT). The costs of the pavement's extra thickness required to carry heavy vehicles and the cost of load-related repairs are allocated based on standard 18-kip (80 kN) single axle load (ESAL) or VMT-weighted ESAL.

In 1982, the Federal Highway Administration (FHWA) conducted the first comprehensive HCAS, under which mechanistic-empirical distress prediction models were developed to estimate the amount of damage that different vehicle classes and the environment cause to the pavement (FHWA 1997). The 1982 HCAS was refined in 1997 and new mechanistic-empirical distress prediction models were developed and used in the current nationwide pavement cost model (NAPCOM) for allocating highway costs (Carey 2001). NAPCOM uses EASL-based models for assessing the relative incremental truck damage. The

1997 HCAS was amended in 2000 to include estimates of air pollution-related costs attributable to highway use by motor vehicles.

At the state level, several state departments of transportation (DOTs) have conducted highway cost allocation studies to address their local highway systems and conditions. The 1999 Arizona Simplified Model for Highway Cost Allocation Studies (Carey 2001) and the Indiana 1983 and 1988 highway cost allocation studies (Fwa *et al*. 1990; Sinha and Fwa 1987) use Federal HCAS procedures, whereas the 1998 and 2007 Oregon cost-responsibility study (Carey 2001; Stowers *et al*. 1999) and the Minnesota 1990 highway cost allocation study (Mn/DOT 1990) use a simplified version of the Federal HCAS procedures. The details of these studies are summarized in Boilé *et al*. (2001).

Generally, highway cost allocation studies have been devised to resolve the complicated distribution of revenues and expenses among different groups of highway users and assess the equity of highway user tax structures (Boilé *et al*. 2001). These studies provide an opportunity for assessing the cost of permit fees for super-heavy loads based on a sound theory. The proposed process in this work applies HCAS principles, in conjunction with new models, to generate realistic estimates of permit fees for heavy loads that is based on the allocation of pavement damage and cost of repair for any given pavement segments.

A rationale process for allocating permit fee is proposed hereby. The practical use of the process is for the policy makers to make more informed decision on the permit fee cost structure. An example of the day-to-day use of this process is described by Tirado *et al*. (2006) where IntPave was linked to a GIS map of the routes in New York State to conduct the damage analysis automatically.

6.3 Permit fee estimation process

Generally, the permit fee for heavy and super-heavy trucks is established to recover administrative costs of issuing the permit, such as load inspection costs and permit processing fee. What is lacking is a formal, yet practical, methodology to aid highway agencies in determining permit fee for super-heavy loads considering the cost of repairing highway infrastructure due to the added damage that these loads cause. A simple allocation cost methodology for estimating the permit fee for these trucks is presented here.

The proposed permit fee is estimated based on the predicted long-term damage caused by heavy loads and on the estimated cost for repairing the deteriorated pavement. The cost of repair is allocated based on the extra damage caused by the passing of a heavy vehicle compared to the damage caused by a standard truck.

The process requires the pavement structural properties as well as the axle and load configurations of both a case (heavy) truck and a user defined standard truck (usually an 80-kip T3S2 truck). As mentioned before these properties are input to IntPave FE module to estimate pavement performance, as previously discussed. The process of permitting can be itemized in the following 10 steps:

1. The variations in damage as a function of truck passes (called the *damage curves* hereafter) are developed for the standard truck and heavy truck to a predefined failure threshold (e.g. 0.5 in. of rutting or 20% of cracking).
2. The number of passes of the standard truck to research the failure threshold is determined as $N_{\text{std: } f.}$
3. The amount of distress after 100 passes of the standard truck, $d_{Nstd:100}$ is estimated from the standard truck damage curve.

4. The number of passes of the heavy truck to cause the same amount of distress, $N_{truck:eq}$, is determined from the heavy truck damage curve.
5. The damage caused by one extra pass of the heavy truck after $N_{truck:eq}$ (called $d_{truck:eq+1}$) is determined from the heavy truck damage curve.
6. The extra number of equivalent standard truck passes beyond 100 passes necessary to cause $d_{truck:eq+1}$ rutting is estimated from the standard truck damage curve (called $\Delta N_{std:eq}$).
7. The percentage of pavement life reduction due to one pass of the heavy truck, *LR*, can be calculated as

$$LR = \frac{\Delta N_{std:eq}}{N_{std:f}} \times 100\% . \tag{6.1}$$

8. The pavement design life in years, n_f, or a lower distress threshold, as a function of the average annual daily truck traffic, *AADTT*, is calculated as

$$n_f = \frac{N_{std:f}}{360 \times AADTT} , \tag{6.2}$$

9. The present-worth value, *PWV*, of repairing the pavement when the failure threshold is reached is then calculated based on the estimated cost of a repair strategy defined by the user, *Cost*, based on the distress limit, and the per annum interest rate, *i*, as

$$PWV = \frac{Cost}{(1+i)^{n_f}} , \tag{6.3}$$

10. The permit fee, *PF*, is simply calculated from

$$PF = PWV \times LR . \tag{6.4}$$

The number of 100 passes was selected for stability of the analyses, as will be shown afterwards; however, the user has the choice of selecting a failure criteria based on acceptable

distress threshold levels above which pavement rehabilitation would be required. This process is summarized with each step marked in the flow chart in Figure 6.1.

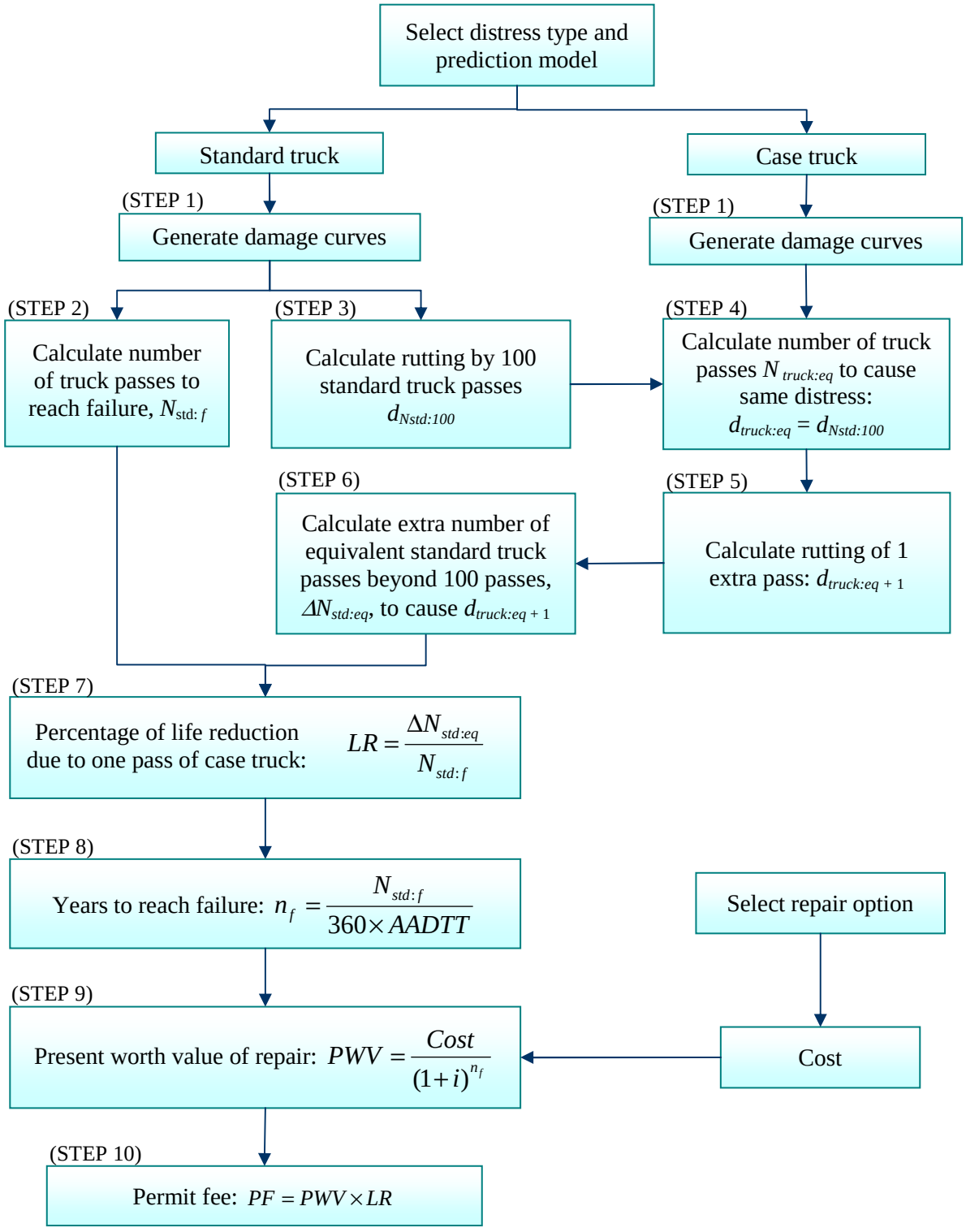

Figure 6.1 - Process for estimating truck permit fees.

6.4 Sample analysis

In this section a case study is presented to illustrate the proposed process. The permit fee for a 160-kip (700 kN) truck is obtained for a representative Texas State Highway system flexible pavement whose properties are shown in Figure 6.2. Since rutting is usually considered the main mode of distress due to heavy loads, the results from that model is shown here. A failure criterion of 0.5 in. rut was set before triggering pavement rehabilitation. Repair methods and typical average unit prices used in this study were obtained from TxDOT's FY 2007 average low bid unit price database (TxDOT 2007a). These unit prices may not necessarily be applicable to other agencies. Axle and load configuration for the 160-kip truck and the standard 80-kip truck are shown in Table 6.1, along with other truck configurations to be used in this case study. Appropriate truck axle configurations were assigned to each load group to fulfill the requirements of Texas Oversize/Overweight Permit Regulations. The maximum weight limits for an axle or axle group are based on the lesser of a 650 lb/in. of tire width or a maximum load of 25 kip (110 kN) for a single axle, 46 kip (200 kN) for a tandem axle, 60 kip (270 kN) for a tridem axle, 70 kip (310 kN) for a quad axle, and 60 kip (270 kN) for trunnion configuration with a total of 16 tires per two axles ((TxDOT 2007b).

HMA	**E = 500 ksi, H = 3 in., ν = 0.33, α = 0.78, μ = 0.25**
Base	**E = 50 ksi, H = 12 in., ν = 0.33, α =0.74, μ = 0.40**
Subgrade	**E = 10 ksi, ν = 0.33, α = 0.90, μ = 0.40**

Figure 6.2 - Control pavement section.

Table 6.1 - Truck configurations considered.

Truck	80-k (Control)	120-k	160-k	200-k	240-k
Steering Axle (lbs)	12,000	12,000	12,000	12,000	12,000
Tandem Axle (lbs)	34,000	38,000	36,000	38,000	36,000
Trailing Axle (lbs)	34,000	70,000	112,000	150,000	192,000
Trailing Axle Type	Tandem	Quad	Trunnion	Trunnion	Trunnion
Truck Configuration					
Empty Vehicle Weight (kips)	33	37	37	41	45
Cargo [Payload] (kips)	47	83	123	159	195

Figure 6.3 shows the rutting curves for the first 120 passes of a 160-kip truck and a standard 80-k T3S2 truck. These rutting curves are shown in Figure 6.4 to failure (0.5 in. of rut). From Figure 6.4, the number of standard truck passes to reach failure is about 0.8 million.

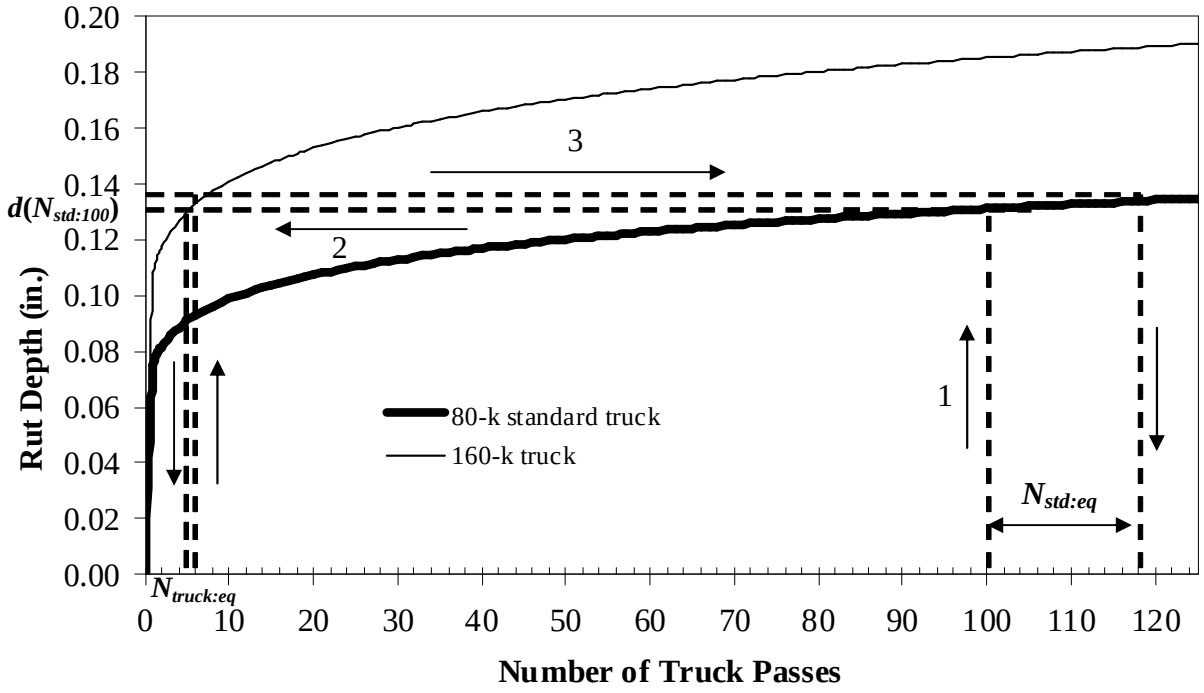

Figure 6.3 - Rutting vs. truck passes for standard and heavy trucks.

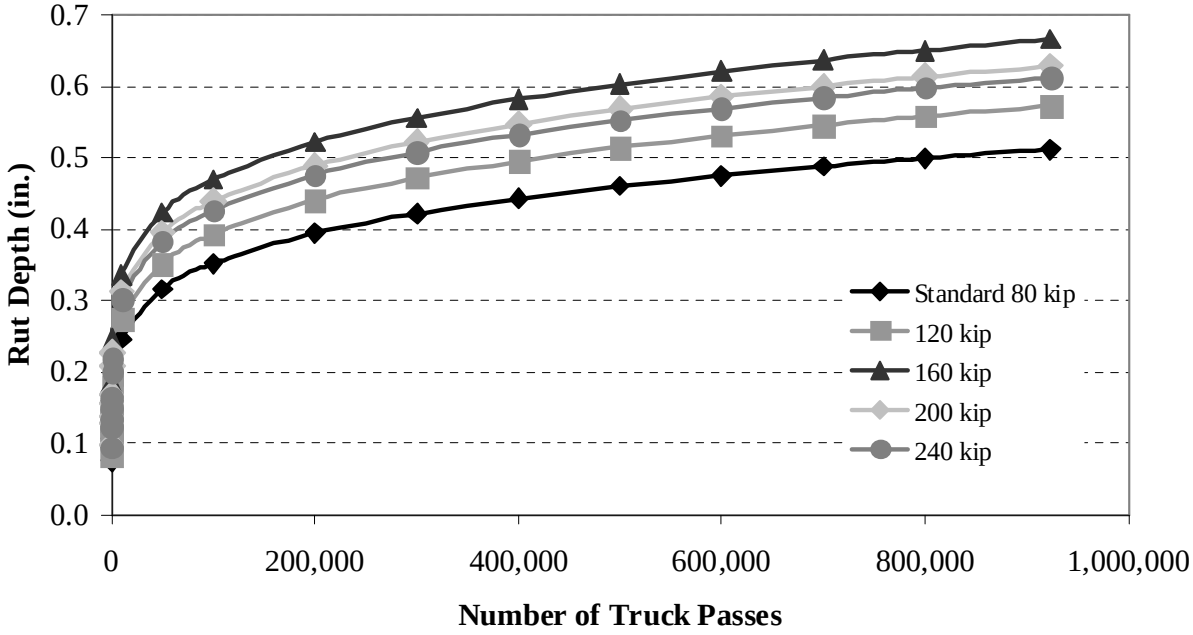

Figure 6.4 - Variations in rut depth with number of passes of standard and several heavy trucks.

From Figure 6.3, the rut depth caused by 100 standard truck passes, $d_{Nstd:100}$, is 131 mils. From the horizontal dashed line marked as 2, the equivalent number of heavy truck passes necessary to reach the same amount of rutting, $N_{truck:eq}$, is 5. The sixth pass of the heavy truck accounts for an extra 27 mils of rutting. The equivalent number of standard truck passes to cause the same 27 mils of rutting, $N_{std:eq}$, is 18 (follow horizontal dashed line marked as 3). Using Equation 6.1, the pavement life reduction due to one pass of such 160-kip truck is 0.0022%. Assuming a pavement design life, n_f, of 5 years after which a mill-and-overlay has to be performed, a repair cost of about $86,000/lane-mi is anticipated. Given a discount rate of 3%, and using Equation 6.4, the permit fee for the 160-kip truck is about $1.62 per lane-mile.

6.5 Parametric studies

The flexible pavement system in Figure 6.2 is considered as the control section. The control truck considered was a standard 80-kip truck as shown in Table 6.1. As shown in Figure 6.4, pavement rehabilitation should be initiated after 0.8 million passes of the control truck, considering an accumulated rut depth of 0.5 in. as the threshold for rehabilitation. Average annual standard truck traffic of 160,000 was assigned as control traffic volume for this case study based on an average period to rehabilitation of five years and adequate design of pavement. The repair strategy considered for this case study is milling 2 in. and a 3 in. overlay, with an assumed average cost of $12.25 /yd^2. A discount rate of 3% is assumed throughout this study.

Four other truck configurations, shown in Table 6.1, were considered as heavy trucks with gross vehicle weights ranging from 120 kip to 240 kip. The variations in the rut depth with the number of passes of the four heavy trucks are also included in Figure 6.4. The rut depths for trucks with GVW's of 200 and 240 kips are less than the 160-kip truck simply because based on

the current interpretation of the legal axle loads, the 160-kip truck legally can exert more pressure per tire than the other two heavier trucks. The truck with a gross vehicle weight of 160 kips was used as the control heavy truck. Unless otherwise noted, this truck is analyzed in this parametric study.

The costs of permit for the four heavy trucks are shown in Figure 6.5. For the control heavy truck the estimated cost is $1.62/mile. Again, this truck yields higher permit fee than trucks with GVW's of 200 and 240 kips because legally the 160-kip truck exert more pressure to the pavement as discussed above.

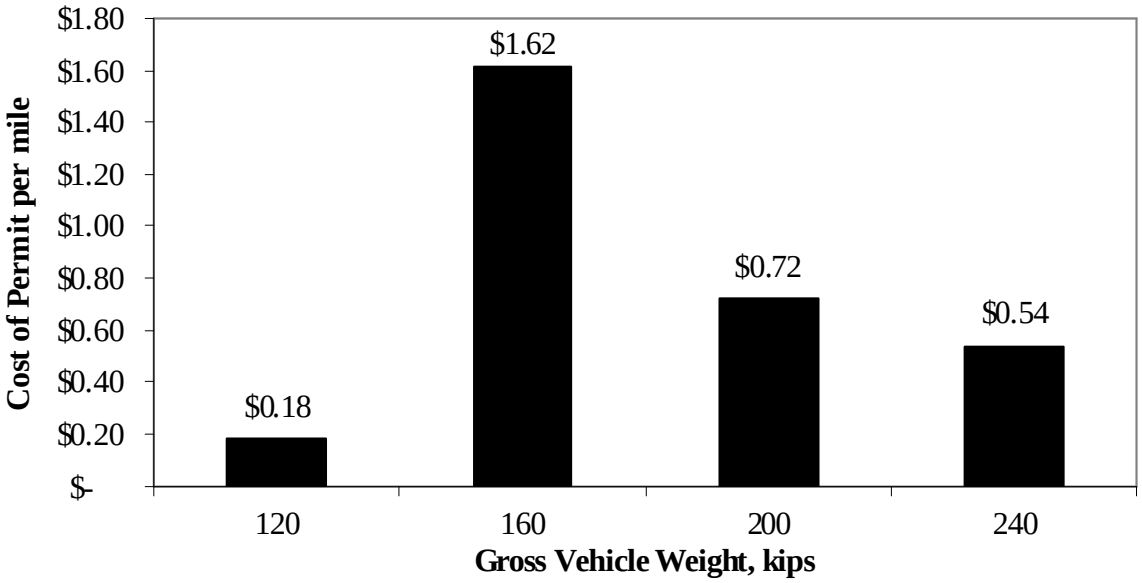

Figure 6.5 - Impact of different heavy trucks on permit cost.

6.5.1 Impact of threshold to rehabilitation

The assumed threshold to rehabilitation has an exponential impact on the cost of permit as shown in Figure 6.6. As the failure threshold increases from 0.3 in. to 0.9 in., the cost of permit decreases from about $36/mile to almost zero. Therefore, the selection of a realistic threshold is necessary.

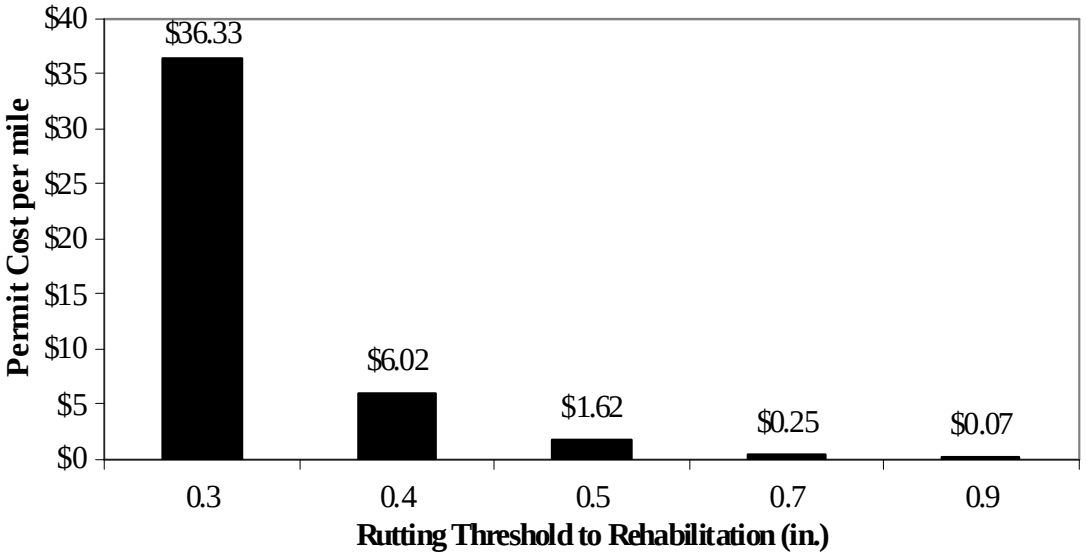

Figure 6.6 - Impact of rutting threshold to rehabilitation on permit cost.

6.5.2 Impact of over/under designing highway

The impact of mis-estmation of traffic volume on the cost of permit was also evaluated. Variations of actual AADT to about 30% more (i.e., time to rehabilitation is reduced to 3 years) and to half of the design AADT (i.e., time to rehabilitation of 10 years) were evaluated. As shown in Figure 8, the cost of permit somewhat decreases as the traffic volume decreases. The trend would reverse if the rate of increase in the cost of construction was greater than the interest rate. The effect of over or under designing the pavement has relatively small impact on permit fee as compared to the impact of rutting threshold to rehabilitation.

Figure 6.7 - Impact of mis-estimation of traffic volume on permit cost.

6.5.3 Impact of pavement structure

For a mechanistic permit cost analysis, the pavement structure plays an important role. For example, the impact of the HMA layer thickness on the permit cost is demonstrated in Figure 6.8a. All other structural parameters were maintained at their control values. For each HMA thickness the volume of traffic was adjusted to yield a period of five years to rehabilitation. The thicker the HMA layer is, the lower the cost of permit will be.

In the same manner, as the thickness of the base increases, the cost of permit increases as well, as shown in Figure 6.8b. This counter-intuitive trend occurs because the control base is not as high a quality as it should be. As the base becomes thicker, the rutting of the base became more sever, even though the rutting of subgrade became less. For comparison purposes, the cost of permit as a function of base thickness for a semi-rigid base (modulus of 225 ksi) is also shown in Figure 9b. In this case, the contribution of base to total rutting is small and the cost of permit decreases to about 10 cents/mile.

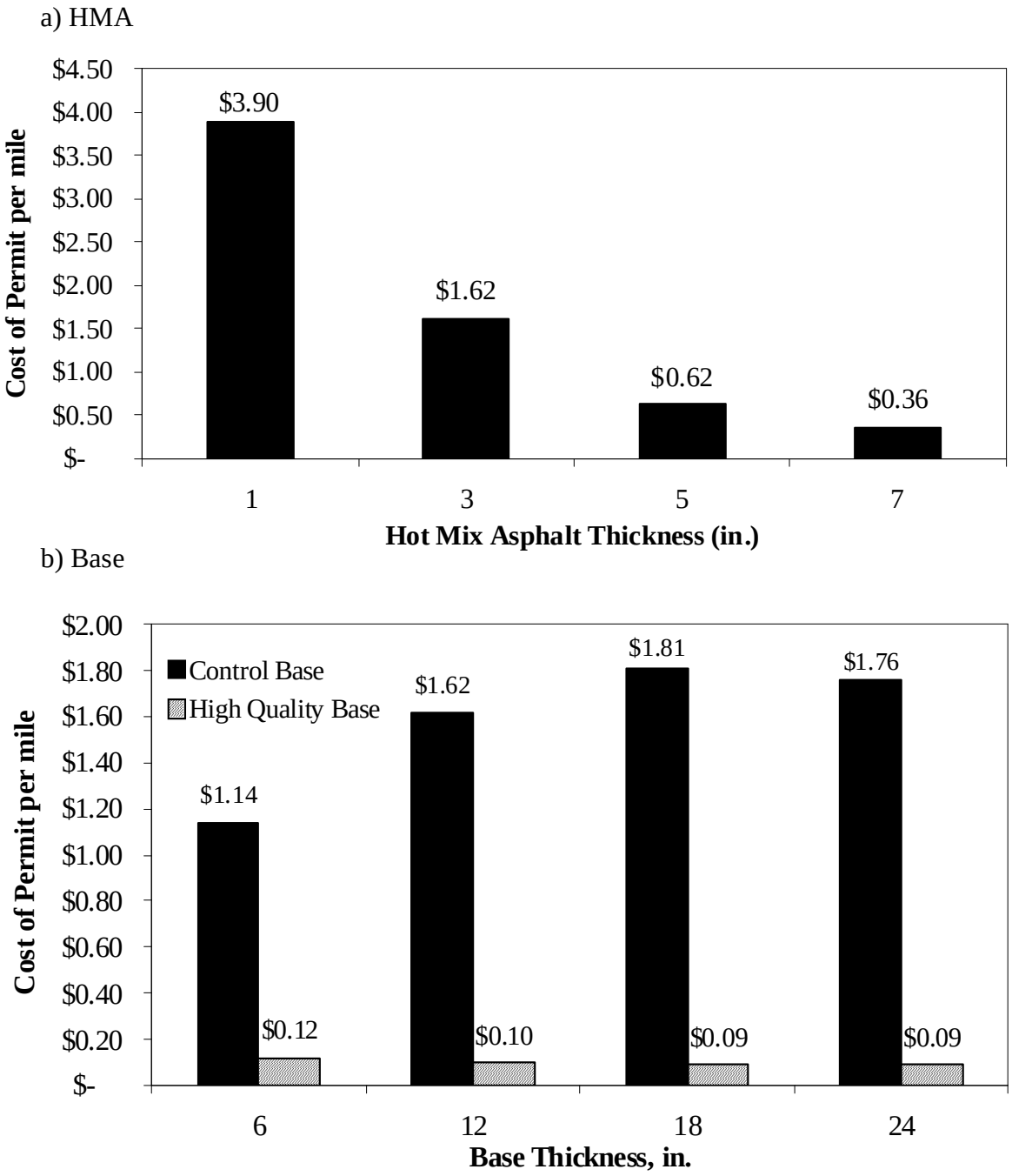

Figure 6.8 - Impact of layer thickness on permit cost.

The moduli of the HMA, base and subgrade are perturbed in Figure 6.9. As the modulus of the HMA increases, the cost of permit decreases (Figure 6.9a). The increase in the modulus of the base has a drastic impact in the cost of permit as well (Figure 6.9b). As the base modulus

decreases from 225 ksi (semi-rigid) to 25 ksi (very low quality) the permit cost increases from 10 cents/mile to over $5/mile. As reflected in Figure 6.9c, the modulus of subgrade is also very important. For a stiff subgrade (modulus of 30 ksi) the cost of permit is about 10 cents/mile, but on a very soft subgrade (modulus of 5 ksi) the cost is near to $30/mile.

6.5.4 Impact of existing damage before passing of heavy truck

All the permit costs discussed so far have been based on the assumption that the heavy truck passes over a new pavement (i.e. after 100 passes of standard truck). However, a heavy truck may pass at any time in the life of the pavement. The existing rutting at the time of the passage of the heavy load impacts the permit fee. The variation in equivalency of one pass of the heavy truck as a function of the number of passes of the standard truck before the passage of the heavy truck is shown in Figure 6.10. The progression of rutting as the function of standard truck passes is shown in Figure 6.11. As the number of passes and as a result the rut depth increases, the number of equivalent standard trucks decreases (for cracking, this pattern may be the opposite). The cost of permit, as shown in Figure 6.12, naturally decreases as the load equivalency decreases to an asymptotic value. Since the designation of the permit fee is a matter of public policy, this type of results can be a guide to the policy makers in deciding on the permit fee.

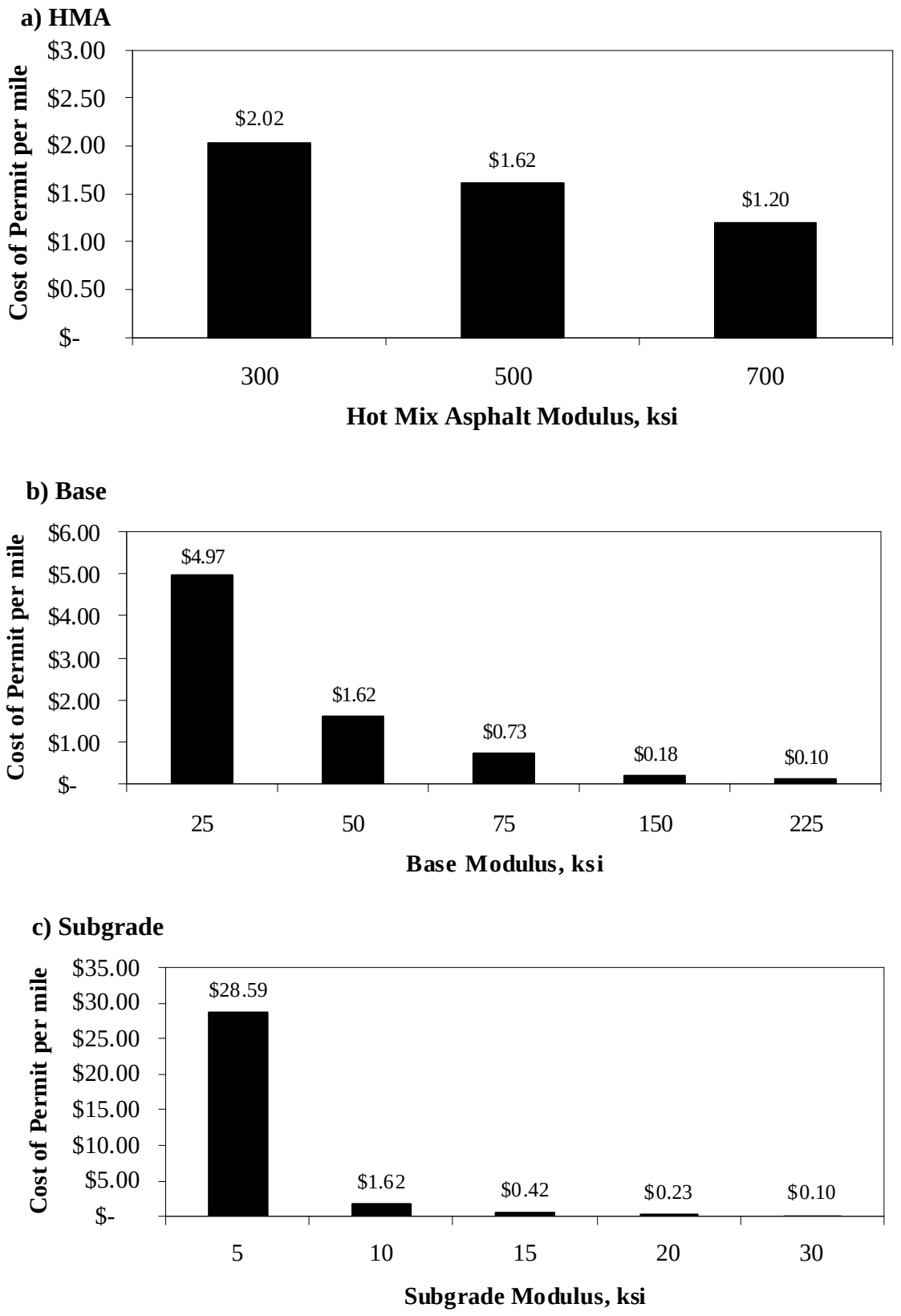

Figure 6.9 - Impact of layer moduli on permit cost.

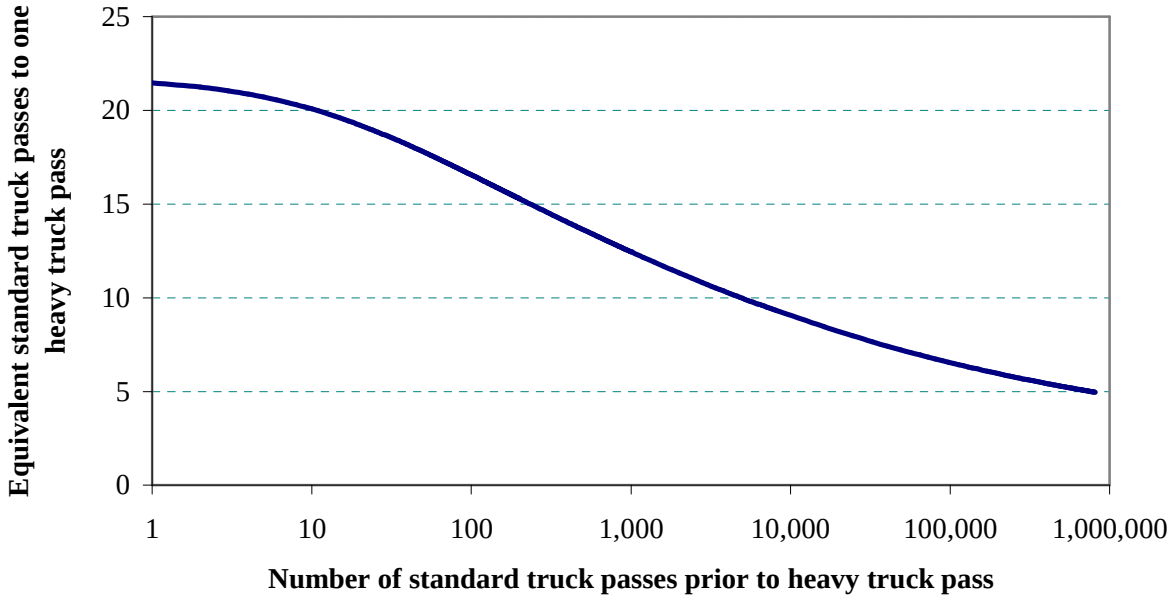

Figure 6.10 - Impact of existing damage on permit fee.

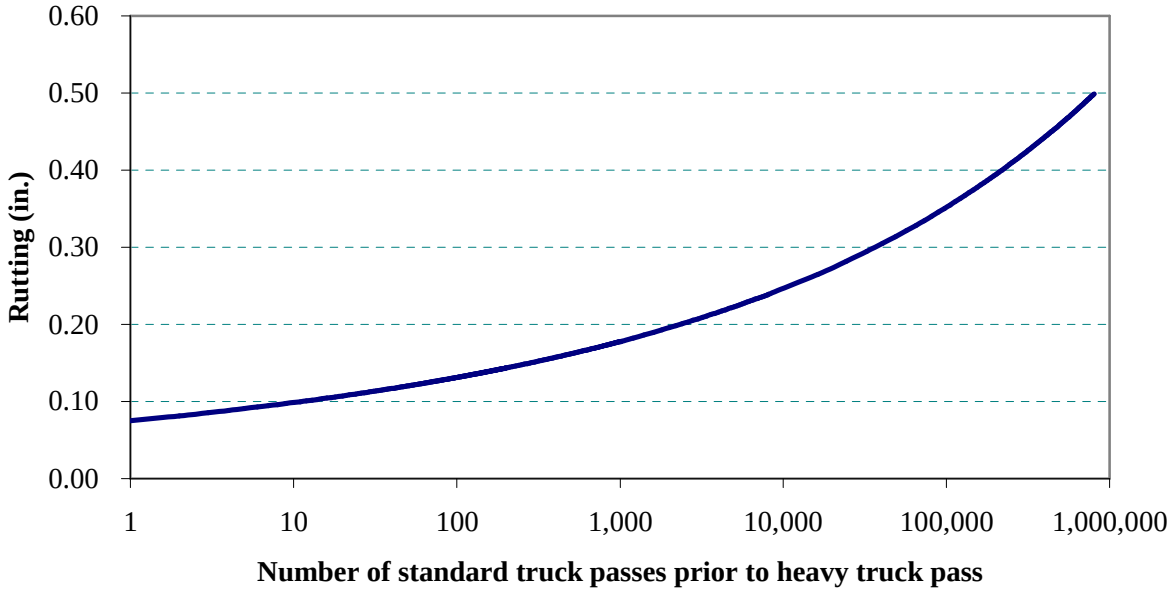

Figure 6.11 - Impact of existing damage on permit fee.

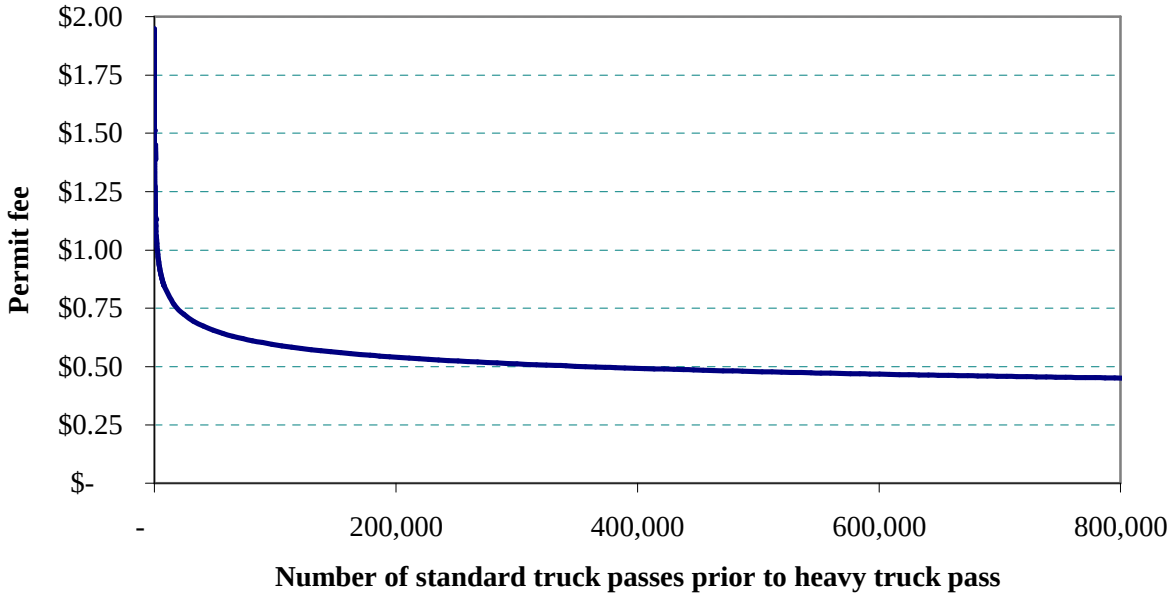

Figure 6.12 - Impact of existing damage on permit fee based on heavy truck pass.

Chapter 7

Summary, Conclusions and Recommendations

7.1 Summary

The objective of this study was to develop a tool suitable for analyzing flexible pavement systems based on finite element analysis optimized for generating a mesh and matrix assemblage suitable for calculating typical pavement distresses caused by truck traffic. The developed tool was called IntPave, an Integrated Pavement Damage Analyzer; a finite element analysis program developed with a graphical user interface suitable for analyzing flexible pavement systems. With the use of such tool the impact of heavy and super-heavy trucks was assessed, according to their axle configurations and pavement structure at a given level of distress and compared to a standard truck. In order to carry out this comparison it a new procedure was proposed to analyze the effect truck traffic on pavement deterioration by integrating the effect of all axles comprising a truck into a truck pass, rather than focusing on axle groups. Moreover, the effect of a truck passage is evaluated with respect to a standard truck to evaluate the extra damage caused by such truck. Such comparative analysis was be used to propose a procedure based on a mechanistic-empirical (M-E) analysis to estimate permit fees based on a truck axle loading and configuration and the predicted pavement deterioration it causes. This procedure is based on the estimation of the incremental damage caused by the heavy truck. This incremental damage is transformed to a permit fee based on the present-worth value of repairing the pavement. Furthermore, by taking advantage of the finite element code already implemented, a time integration technique was

developed as a tool for simulating wave propagation suitable for assessing seismic non-destructive testing.

7.2 Conclusions

Case studies were presented based on typical highway pavements to determine damage factors based on the number of truck passes to reach failure in rutting and compare them to damage factors based on traditional AASHTO load equivalency factors. Based on the study carried out the following conclusions can be made:

- Traditional equivalency approach had limitations when evaluating damage as they fail to consider the load characteristics such as number of tires per axle, tire spacing, and complex axle configurations. As a consequence, in some cases these factors tend to be mis-estimated.
- Overloaded vehicles that are not within the overload permit policies do greatly increase pavement deterioration as proven by all approaches for damage equivalencies.
- A parametric study was carried to demonstrate the sensitivity of the cost of the permit fee to the gross vehicle weight and axle configurations, threshold to rehabilitation, traffic volume, and pavement structure moduli properties and thicknesses.
- Assigning permit fees to the passage of heavy loads on a highway network is rather complex and impacted by a number of interacting parameters.
- The more substantial the pavement structure is, the lower the incremental damage and as a result the permit fee will be.

- The most critical layer in the pavement for reasonably stiff subgrades is the base layer. The higher the quality of the base is, the less the permit fee will be. Thicker lower quality base promotes more incremental damage and as a result higher permit fee.
- The damage to the pavements when the subgrade is extremely soft is significant, and as such the hauling of heavy load on such roads should not be permitted.
- The policies of a local highway agency in terms of the damage threshold to rehabilitation have a significant impact on the permit fee. The more relaxed this threshold is, the lower the cost of permit will be.
- Unlike for the actual pavement design, the uncertainty in the traffic volume has a small impact in the cost of the permit for passage of a heavy load.
- The existing pavement damage at the time of the passage of the heavy load also impacts the permit fee, and may be considered.

7.3 Recommendations

The following recommendations were derived from this study:

- A further study on the sensitivity of α and μ rutting parameters must be carried as it was found that these parameters, specifically the rate of increase in permanent deformation against the number of load applications, α, can make a significant impact on rutting and, as a consequence, in damage equivalencies.
- The effect of gross vehicle weight and axle configurations on damage and the cost of permit fee were analyzed; however, tire pressure is another factor that still must be taken into consideration for further study. Though the load exerted by tires might be the same, the pressure can be different, as the tires inflict the same weight on a different area, as

long as the pressure is within requirements. However, varying pressure does have an effect on how soon failure is attained.

- The effect of the time of passage of the heavy load on the permit fee was analyzed for one type of distress, i.e. rutting; however, a further study on the effect of the time of passage must be carried on for fatigue cracking. A combination of the both major structural distresses should also be considered.
- Implementation of linear quadrilateral elements on the dynamic analysis proved suitable for analyzing the wave propagation problem; however, small-sized elements are required. Higher-order elements, such as spectral elements, can be implemented to overcome this problem, with the purpose of improving the analysis by attaining better accuracy and reducing computation time.

References

AASHO. (1961). "The AASHO Road Test: History and Description of the Project." *61A*, AASHO.

AASHTO. (1993). *AASHTO guide for design of pavement structure*, American Association of State Highway and Transportation Officials, Washington, DC.

Aouad, M. F., Stokoe II, K. H., and Briggs, R. C. (1993). "Stiffness of Asphalt Concrete Surface Layer from Stress Wave Measurements." Transportation Research Record: Journal of the Transportation Research Board, Transportation Research Board of the National Academies, Washington, D.C., 29-35.

Barksdale, R. D., Alba, J. L., Khosla, N. P., Kim, R., Lambe, P. C., and Rahman, M. S. (1997). "Laboratory determination of resilient modulus for flexible pavement design: Final report." *Georgia Tech Project E20-634*, Federal Highway Administration, United States Department of Transportation, Washington, District of Columbia.

Bathe, K.-J., and Wilson, E. L. (1976). *Numerical Methods in Finite Element Analysis*, Prentice-Hall, Inc., Englewood Cliffs, NJ.

Bay, J. A., and Stokoe II, K. H. (1990). "Field Determination of Stiffness and Integrity of PCC Slabs using the SASW Method." Nondestructive Evaluation of Civil Structures and Materials Conference, University of Colorado, Boulder., 71-86.

Belytschko, T. (1983). "An Overview of Semidiscretization and Time Integration Procedures." Computational Methods for Transient Analysis, T. B. a. T. J. R. Hughes, ed., North Holland, Amsterdam, 1-65.

Blab, R., and Harvey, J. T. (2002). "Modeling Measured 3D Tire Contact Stresses in a Viscoelastic FE Pavement Model." *International Journal of Geomechanics*, 2(3), 271-290.

Boilé, M., Ozbay, K., and Narayanan, P. (2001). "Infrastructure Costs Attributable to Commercial Vehicles." FHWA, Center for Advanced Infrastructure & Transportation, Rutgers, The State University of New Jersey.

Carey, J. (2001). "Implementation of the Simplified Arizona Highway Cost Allocation Study Model. ." Arizona Department of Transportation, FHWA, U.S. Department of Transportation.

Chen, D.-H., Zaman, M., Laguros, J. G., and Soltani, A. (1995). "Assessment of Computer Programs for Analysis of Flexible Pavement Structure." *Transportation Research Record: Journal of the Transportation Research Board*, 1482, 123-133.

Cho, Y. S. (2003). "Non-destructive testing of high strength concrete using spectral analysis of surface waves." *NDT & E International*, 36(4), 229-235.

Cho, Y. S., and Lin, F.-B. (2005). "Spectral analysis of surface waves in single and multi-layer slabs with finite thickness using finite element modelling." *NDT & E International*, 38, 195-202.

Cook, R. D., Malkus, D. S., Plesha, M. E., and Witt, R. J. (2001). *Concepts and Applications of Finite Element Analysis*, John Wiley & Sons, Inc.

CyberLogic, Inc. (1999). "Wave2000® Ver. 1.00 User Guide & Reference Manual." CyberLogic, Inc., New York.

Desai, C. S. (2001). "User's Manual for the DSC-2D Code for the 2002 Design Guide." Arizona State University, Tempe, AZ.

Drnevich, V. P., Kim, S.-I., Alexander, D. R., and Kohn, S. D. (1985). "Spectral Analysis of Surface Waves in Pavement Systems with Random Noise Excitation." Society of Exploration Geophysicists Technical Program Expanded Abstracts; 55th Annual Meeting, Society of Exploration Geophysicists, Tulsa, Oklahoma, 143-145.

Duncan, J. M., Monismith, C. L., and Wilson, E. L. (1968). "Finite Element Analyses of Pavements." *Highway Research Record*, 228, 18-33.

ECONorthwest. (2007). "Highway Cost Allocation Study 2007-2009 Biennium." Oregon Department of Administrative Services, Office of Economic Analysis.

ERES Consultants, Inc. (2004). "Guide for mechanistic-empirical design of new and rehabilitated pavement structures." *Final report – NCHRP Project 1-37A*, National Cooperative Highway Research Program, Transportation Research Board, National Research Council, Washington, DC.

Ewing, W. M., Jardetzky, W. S., and Press, F. (1957). *Elastic Waves in Layered Media*, McGraw-Hill Book Company, Inc., New York.

FHWA. (1997). "1997 Federal Highway Cost Allocation Study: Final Report. ." FHWA, U.S. Department of Transportation.

FHWA. (2003). "VESYS 5Ws User Manual." Office of Infrastructure Research and Development, FHWA, U.S. Department of Transportation.

Fwa, T. F., Sinha, K. C., and Saha, S. K. (1990). "Update Analysis of Highway Cost Allocation." Transportation Research Record: Journal of the Transportation Research Board, Transportation Research Board of the National Academies, Washington, D.C., 1-11.

Ganji, V., Gucunski, N., and Maher, A. (1997). "Detection of underground obstacles by SASW method - numerical aspects." *Journal of Geotechnical and Geoenvironmental Engineering*, 123(3), 212-219.

Ganji, V., Gucunski, N., and Nazarian, S. (1998). "Automated Inversion Procedure for Spectral Analysis of Surface Waves." *Journal of Geotechnical and Geoenvironmental Engineering*, 124(8), 757-770.

Gucunski, N. (1991). "Generation of low frequency Rayleigh waves for the Spectral-Analysis-of-Surface-Waves method," Ph.D. Dissertation, The University of Michigan, Ann Arbor, Michigan.

Gucunski, N., and Shokouhi, P. (2005). "Wavelet Transforms in Surface Wave Analysis." *Soil Dynamics Symposium in Honor of Professor Richard D. Woods*, 159(2), 17.

Hall, K. T., Darter, M. I., and Kuo, C.-M. (1989). "Rehabilitation of Concrete Pavement, Vol. 3, Concrete Pavement Evaluation and Rehabilitation System, Vol. 3, Concrete Pavement Evaluation and Rehabilitation System." *FHWA-RD-88-073*, Federal Highway Administration.

Harichandran, R. S., Yeh, M.-S., and Baladi, G. Y. (1990). "MICH-PAVE: A Nonlinear Finite Element Program for Analysis of Flexible Pavements." Transportation Research Record: Journal of the Transportation Research Board, Transportation Research Board of the National Academies, Washington, D.C., 121-131.

Hossain, M., and Wu, Z. (2002). "Finite Element Simulation of Rutting on Superpave Pavements." 9th International Conference on Asphalt Pavements, International Society for Asphalt Pavements, Copenhagen, Denmark.

Huang, Y. H. (2004). *Pavement Analysis and Design*, Prentice Hall, Upper Saddle River, NJ.

Kenis, W. J. (1977). "Predictive Design Procedures, VESYS Users Manual." *FHWA A-RD-77-154*, Federal Highway Administration.

Kuo, C.-M., and Chou, F.-J. (2004). "Development of 3-D Finite Element Model for Flexible Pavements." *Journal of the Chinese Institute of Engineers*, 27(5), 707-717.

Luke, B. A., and Stokoe II, K. H. (1998). "Application of SASW Method Underwater." *Journal of Geotechnical and Geoenvironmental Engineering*, 124(6), 523-531.

Lysmer, J. (1970). "Lumped mass method for Rayleigh waves. , 43: 17-34." *Bulletin of the Seismological Society of America*, 43, 17-34.

Lysmer, J., and Drake, L. A. (1972). "A Finite Element Method for Seismology." *Methods in Computational Physics*, 11, Seismology: Surface waves and earth oscillations, 181-216.

Lysmer, J., and Waas, G. (1972). "Shear Waves in Plane Infinite Structures." *Journal of the Engineering Mechanics Division*, 98(1), 85-105.

Miller, G. F., and Pursey, H. (1955). "On the Partition of Energy between Elastic Waves in a Semi-Infinite Solid." *Proceedings of the Royal Society of London. Series A, Mathematical and Physical Sciences*, 233(1192), 55-69.

Mn/DOT. (1990). "Result of the Minnesota Highway User Coast Allocation Study." Minnesota Department of Transportation, St. Paul, MN.

Mulungye, R. M., Owende, P. M. O., and Mellon, K. (2005). "Analysis of Response of Flexible Pavements Using Finite Element Methods." *Institute of Technology Blanchardstown Journal*(12), 40-52.

Mulungye, R. M., Owende, P. M. O., and Mellon, K. (2006). "Determining the Effect of Tyre Pressure, Axle Load and Wheel Configuration on Flexible Pavements Fatigue Life using

Finite Element Method." Applied Simulation and Modelling, M. H. Hamza, ed., Rhodes, Greece, 562.

Mulungye, R. M., Owende, P. M. O., and Mellon, K. (2007). "Finite element modelling of flexible pavements on soft soil subgrades." *Materials and Design*, 28, 739–756.

Nazarian, S. (1984). "In Situ Determination of Soil deposits and Pavement Systems by Spectral Analysis of Surface Waves Method," Ph.D. Dissertation, The University of Texas at Austin, Austin, TX.

Nazarian, S., Baker, M. R., and Crain, K. (1993). "Development and Testing of a Seismic Pavement Analyzer." *SHRP-H-375*, Center for Geotechnical and Highway Materials Research, Washington, D.C.

Nazarian, S., and Stokoe, K. H. (1983). "Evaluation of Moduli and Thicknesses of Pavement Systems by Spectral-Analysis-of-Surface-Waves Method." Center for Transportation Research, The University of Texas at Austin, Austin, Texas.

Nazarian, S., and Stokoe, K. H. (1985). "In Situ Determination of Elastic Moduli of Pavement Systems by Spectral-Analysis-of-Surface-Waves Method: Practical Aspects." Center for Transportation Research, The University of Texas at Austin, Austin, Texas.

Nazarian, S., and Stokoe, K. H. (1986). "In Situ Determination of Elastic Moduli of Pavement Systems by Spectral-Analysis-of-Surface-Waves Method: Theoretical Aspects." Center for Transportation Research, The University of Texas at Austin, Austin, Texas.

NRC. (2002). "Regulation of Weights, Lengths and Widths of Commercial Motor Vehicles: Special Report 267." Transportation Research Board of the National Academies, National Research Council, Washington, D.C.

Ritchie, S. G., Yeh, C.-I., Mahoney, J. P., and Jackson, N. C. (1986). "Development of an Expert System for Pavement Rehabilitation Decision Making." *Transportation Research Record: Journal of the Transportation Research Board*, 1070, 90-103.

Rix, G. J. (1988). "Experimental Study of Factors Affecting the Spectral-Analysis-of-Surface-Waves Method," Ph.D. Dissertation, The University of Texas at Austin, Austin, TX.

Rix, G. J., Bay, J. A., and Stokoe II, K. H. (1990). "Assessing In Situ Stiffness of Curing Portland Cement Concrete with Seismic Tests." *Transportation Research Record: Journal of the Transportation Research Board*, 1084, 8-15.

Saad, B., Mitri, H., and Poorooshasb, H. (2005). "Three-Dimensional Dynamic Analysis of Flexible Conventional Pavement Foundation." *Journal of Transportation Engineering*, 131(6), 460-469.

Saad, B., Mitri, H., and Poorooshasb, H. (2006). "3D FE Analysis of Flexible Pavement with Geosynthetic Reinforcement." *Journal of Transportation Engineering*, 132(5), 402-415.

Saliba, J. E. (1990). "Elastic-viscoplastic finite-element program for modeling tire/soil interaction." *Journal of Aircraft*, 27(4), 350-357.

Sánchez-Salinero, I. (1987). "Analytical Investigation of Seismic Methods Used for Engineering Applications," Dissertation, The University of Texas at Austin, Austin, TX.

Sinha, K. C., and Fwa, T. F. (1987). "A Highway Cost Allocation Analysis at the State Level." *Transportation Quarterly*, 41(3), 347-364.

Sivakumar, B., Moses, F., Fu, G., and Ghosn, M. (2007). "Legal Truck Loads and AASHTO Legal Loads for Posting." Transportation Research Board.

Stein, S., and Wysession, M. (2003). *An Introduction to Seismology, Earthquakes, and Earth Structure*, Blackwell Publishing.

Stokoe II, K. H., and Nazarian, S. (1983). "Effectiveness of ground improvement from spectral analysis of surface waves." Eighth European Conference on Soil Mechanics and Foundation Engineering, A.A. Balkema, Helsinki, Finland., 91-94.

Stokoe II, K. H., Nazarian, S., Rix, G. J., Sánchez-Salinero, I., Sheu, J.-C., and Mok, Y.-J. (1988). "In Situ Seismic Testing of Hard-to-Sample Soils by Surface Wave Method." Earthquake Engineering and Soil Dynamics II—Recent Advances in Ground-Motion Evaluation, J. L. V. Thun, ed., American Society of Civil Engineers, Park City, Utah, 264-278.

Stowers, J. R., Reno, A. T., Balducci, P., Mingo, R. D., Wolff, H., Cohen, H., and Haling, D. (1999). "Oregon Highway Cost Allocation Study." State of Oregon, Department of Administrative Services.

Thompson, M. R. (1989). "ILLI-PAVE Based NDT Analysis Procedures." First International Symposium on Nondestructive Testing of Pavements and Backcalculation of Moduli, American Society of Testing Materials, Baltimore, Maryland, 487-501.

Tirado, C., Carrasco, C., Nazarian, S., and Osegueda, R. (2007). "Updates To Software for Estimating Damage due to Superheavy Loads." Center for Transportation Infrastructure Systems, The University of Texas at El Paso, El Paso, Texas.

Tirado, C., Qing, Y., Carrasco, C., Nazarian, S., and Osegueda, R. (2006). "A GIS Based Algorith for Estimating Damage due to Superheavy Loads." Center for Transportation Infrastructure Systems, The University of Texas at El Paso, El Paso, Texas.

Tutumluer, E., and Thompson, M. R. (1997). "Anisotropic Modeling of Granular Bases in Flexible Pavements." *Transportation Research Record: Journal of the Transportation Research Board*, 1577, 18-26.

TxDOT. (2007a). "Average Low Bid Unit Price database for 2006-2007." Texas Department of Transportation.

TxDOT. (2007b). "Oversize/Overweight Permit Rules and Regulations. 43 Texas Administrative Code Chapter 28, Subchapters A – H." T. D. o. Transportation., ed., Motor Carrier Division.

Uddin, W., and Ricalde, L. (2000). "Nonlinear Material Modeling and Dynamic Finite Element Simulation of Asphalt Pavements." Fourteenth Engineering Mechanics Conference, J. L. Tassoulas, ed., American Society of Civil Engineering, Austin, Texas, 6.

Uzan, J. (1989). "JULEA Linear Elastic Analysis Computer Program." US Army Waterways Experiment Station, Vicksburg, Mississippi.

Washington Asphalt Pavement Association, I. (2002). "The Washington Asphalt Pavement Association (WAPA) Asphalt Pavement Guide." Washington Asphalt Pavement Association, Inc., Seattle, WA.

Werkmeister, S., Numrich, R., Dawson, A. R., and Wellner, F. (2003). "Design of Granular Pavement Layers Considering Climatic Conditions." *Transportation Research Record: Journal of the Transportation Research Board*, 1837, 61-70.

White, T. D., and Zaghloul, S. M. (1994). "Guidelines for Permitting Overloads. Part 1. Effect of Overloaded Vehicles on the Indiana Highway Network. Final Report." Federal Highway Administration, U.S. Department of Transportation, Washington, D.C.

WSDOT. (1996). "Legal Load Limits, Overweight Loads and Pavements and Bridges." Washington State Department of Transportation, Olympia, WA.

Zaghloul, S. M., and White, T. D. (1993). "Use of a Three-Dimensional, Dynamic Finite Element Program for Analysis of Flexible Pavement." *Transportation Research Record: Journal of the Transportation Research Board*, 1388, 60-69.

Zhou, F., and Scullion, T. (2002). "VESYS5 rutting model calibrations with local accelerated pavement test data and associated implementation." *Report No. 9-1502-01-2*, FHWA, U.S. Department of Transportation, Texas Transportation Institute, College Station, TX.

Zienkiewicz, O. C. (1977). *The Finite Element Method*, McGraw-Hill, New York.

Curriculum Vita

César C. Tirado Díaz, was born on February 24, 1975 in Mexico City, D.F., Mexico. The only child of César V. Tirado Villegas and Guillermina Díaz Mendoza, he graduated from Escuela Secundaria y Preparatoria de la Ciudad de México, Mexico City, D.F., Mexico, in 1993. He received his Bachelor of Science in Civil Engineering degree from The University of Texas at El Paso in 1996. He received his Master of Science in Civil Engineering degree in 1999 from the same university while working as graduate research assistance at the FAST Center for Structural Integrity and Aerospace Systems. He worked in the construction industry in Ciudad Juarez before pursuing doctoral studies in civil engineering at UTEP. While pursuing his degree, he worked as a graduate research associate for the Center of Transportation Infrastructure Systems (CTIS) at UTEP.

Permanent Address: 2200 Corley Dr. Apt. 9-B.
Las Cruces, NM, 88001.